NTNU – Trondheim
Norwegian University of
Science and Technology

A novel Characterization Method for electric Properties of single Silver-coated Polymer Spheres

August Emil Tobiesen Stokkeland

Nanotechnology
Submission date: June 2015
Supervisor: Jianying He, KT
Co-supervisor: Helge Kristiansen, Conpart AS
Sigurd Rolland Pettersen, KT

Norwegian University of Science and Technology
Department of Structural Engineering

ABSTRACT

The electrical properties of isotropic conductive adhesives (ICAs) are dependent on the filler concentration and electrical properties of the conductive additives. ICAs with metal-coated polymer spheres (MPS) are an efficient way of reducing the amount of precious metals in the adhesive without compromising the condcuting properties. Today little is known about the electrical properties of a single MPS and how the thickness of the metal coating relates to the electrical properties, because no good method exists for measuring electrical properties of spherical thin films of small diameters.

In this work, a method for probing silver-coated polymer spheres with micromanipulators, is developed and tested. The measurements were done in a dual beam focused ion beam (FIB)/scanning electron microscope (SEM) with a large vacuum chamber, allowing for manipulation and observation in the nanometer range. Polycrystalline tungsten probes are used for the measurements. They are shaped into flat punch probes with an ion beam and controlled by micromanipulators.

Electrical measurements with both two and four probes/wires were performed, the latter found to give precise measurements of the silver coating investigated: The slope of the measured voltage drop divided by the total current was found, V/I, for simplicity called *resistance* throghout this study. The resistance decrease monotonically with increasing coating thickness. From 0.604 Ω for the 60 nm thick coating, to 0.118 Ω, 0.096 Ω, and 0.079 Ω for the 100 nm, 150 nm, and 270 nm respectively. Computer simulations of the same system conducted with *COMSOL Multiphysics*, supports the experimental findings. The simulations have resulted in a resistivity prediction model, which predicts the silver coating resistivity given the sphere's geometry and measured resistance.

The proposed method proves it possible to conduct measurements on single micron sized silver-coated polymer spheres with a high precision. The promising method lays the foundation for further development of the four-wire setup in addition to even better understanding of the silver coatings.

SAMMENDRAG

De electriske egenskapene til isotropt elektrisk ledende lim (isotropic conductive adhesives, ICA) er avhengig av konsentrasjonen av iblandet ledende materiale og det ledende materialets elektriske egenskaper. ICAer av metallpletterte polymerkuler har vist seg å være svært effektive i å få ned mengden edle metaller, uten at det går på bekostning av limets strømledende egenskaper. Det finnes i dag lite kunskap om metallpletterte polymerkuler og hvordan pletteringstykkelsen påvirker de elektriske egenskapene deres. Dette er fordi det ikke finnes noen god måte å undersøke de elektriske egenskapene til slike sfæriske tynnfilmer med liten diameter.

Dette arbeidet tar for seg å utvikle og teste en metode for å utføre målinger på metallpletterte polymerkuler ved hjelp av mikromanipulatorer. Målingene er utført i et kombinert sveipeelektornmikroskop (SEM) og fokusert ionestråle (FIB) med et stort vakuumkammer, som gir mulighet for både å manipluere og observere på nanometerskala. Prober av polykrystallinsk wolfram ble brukt under målingene. De ble slipt ned til en flat kontakflate av ionestrålen og ellers kontrollert av mikromanipulatorene.

Det ble utført målinger med både to og fire prober. Målingene med fire prober viste seg å være mest presise: Det ble funnet verdier for stigningstallet til spenningsfallet delt på den totale strømmen V/I, for enkelhets skyld kalt *motstand*, Ω, i denne studien. Motstanden viste seg å synke monotont ved økende pletteringstykkelse. Fra 0.604 Ω for den 60 nm tykke pletteringen, til henholdsvis 0.118 Ω, 0.096 Ω og 0.079 Ω for 100 nm, 150 nm og 270 nm pletteringene. Det ble laget datamodeller av samme oppsett i *COMSOL Multiphysics* som støttet de experimentelle funnene. Disse modellene la grunnlaget for en modell for å forutsi en metallplettert polymerkules resistivitet ut fra geometriske konstanter og målt motstand.

Den foreslåtte metoden har vist at det er mulig å gjennomføre presise målinger på en enkelt metallplettert polymerkule. Dette legger grunnlaget for videre utvikling av målemetoden med fire prober, samt en bedre forståelse av de elektriske egenskapene til sfæriske sølvpletteringer på mikrometerskala.

PREFACE

This report is the result of a study towards a master's degree in nanotechnology at the Norwegian University of Science and Technology (NTNU) during the spring 2015. The study is a continuation of a preliminary study done in the fall 2014, and it is a collaboration between the Nanomechanical Lab at the Department of Structural Engineering and their industry partner Mosaic Solutions AS under the supervision of Ass. Prof. Jianying He and Dr. Helge Kristiansen respectively.

The experimental part of the project have to a large extent been performed in the FIB/SEM, NTNU NanoLab. The Research Council of Norway is acknowledged for the support to NTNU NanoLab through the Norwegian Micro- and Nano-Fabrication Facility, NorFab and for founding through project number 225962/E20, *Novel Conductive Adhesives Technology Platform for Solar Industry*. Thanks to technical engineer Ken Roger Ervik for help and assistance with the FIB/SEM and miBots. I would also like to thank Ph.D. cand. Vidar Tonaas Fauske from the Department of Physics for writing the sourcemeter script.

I would also like to thank Prof. Zhiliang Zhang for help with the COMSOL Multiphysics software and Ass. Prof. Jianying He for guidance and feedback, keeping my eyes set on the task. A special thanks to Ph.D. cand. Sigurd Rolland Pettersen for assistance, discussions and feedback throughout the whole study. Finally, I would like to thank familiy and friends for their support during my study and master's work.

CONTENTS

ACRONYMS

60Ag	Silver-coated polymer spheres with a silver coating of 60 nm
100Ag	Silver-coated polymer spheres with a silver coating of 100 nm
150Ag	Silver-coated polymer spheres with a silver coating of 150 nm
270Ag	Silver-coated polymer spheres with a silver coating of 270 nm
Ag	Silver
AgPS	silver coated polymer sphere
AFM	Atomic Force Microscope
BSE	Backscattered Electrons
CC	Carbon Cement
CMY	Cooper-Mikic-Yovanovich
ECA	electrical conductive adhesives
EMFP	Electon Mean Free Path
FEG	Field Emission Gun
FEM	Finite Element
FIB	Focused Ion Beam
Ga	gallium
I-V	Current-Voltage
IC	Integrated circuit
ICA	isotropic conductive adhesive
LIMS	liquid ion metal source

miBot	micro manipulator
PDE	Partial Differential Equation
PMMA	Poly(methyl methacrylate)
QNM	Quantitative Nanomechanical Mapping
RMS	Root Mean Square
SE	Secondary Electrons
SEM	Scanning Electron Microscope
StEM	standard error of the mean
Si	silicon
AgO	silver(II) oxide
W	tungsten
Z	atom number

1 INTRODUCTION

Integrated circuits (ICs) are today the foundation of all modern electronic products. But the ICs themselves do not form a complete system, they have to be connected with other components into a system-level board. The requirements for these interconnections are increasing with regard to specific electrical, mechanical and thermal properties. In the eventuality of the phasing out of the lead-bearing solders, electrical conductive adhesives (ECA) are one of the promising new environment friendly alternatives [1, chap. 1]. ECAs consists of an organic and/or polymeric binder with a conductive filler. The fillers are often flakes of precious metals, where the amount and type of metal controls the conductivity. To have the same isotropic conductive properties like conventional solder, an isotropic conductive adhesive (ICA) would have to be filled with a high concentration of metal flakes. A high concentration of precious metal is expensive, and the current research focus on the reduction of the amount of metal while retaining the conductive properties [2]. Copper and other non-noble metals develop an insulating oxide layer upon ageing, making them unsuitable. Silver on the other hand, develop a layer of conductive silver oxide, and is for that reason preferred [1, chap. 4.1.3.1] and well known in the electronic packaging field. Conductive fillers based on monodisperse polymer spheres coated with a thin silver film are therefore developed by Conpart AS [3]. These silver coated polymer sphere (AgPS) retain a large metal surface area, while considerably reducing the amount of silver.

The use of silver-coated polymer spheres in ICAs is a novel application, and the properties of the AgPS as a conductive filler are under investigation [4–6]. The conductivity is a key aspect of an ICA and can be divided into three different contributions from the conductive filler: The concentration of the conductive filler, the contact area between the filler particles, and the resistance over one single filler particle.

The concentration of fillers do as mentioned, play an important part. According to the percolation theory of conduction[1, chap. 4.1.1], the resistivity of an ICA drops drastically from being an insulator to be

a conductor over a critical filler concentration. The ICAs with AgPS have been tested to compare the conductivity with silver flake fillers. Equal conductivity is achieved by using just one quarter of the volume fraction of silver [2], but at the same time doubling the total amount of filler to almost 50 vol%. Therefore, the change in composition of the conductive adhesive and how it affects the mechanical properties, has been tested. When comparing the mechanical properties of ICAs with AgPS filler against silver flakes, the AgPS filler proves to give a stronger and more ductile adhesive [7].

The contact resistance between the spheres is not investigated thoroughly, but a theoretical model to calculate the resistivity over a deformed metal-coated polymer sphere exists for anisotropic conductive adhesives [8]. However, this model does not take into account the small deformations applicable to isotropic conductive adhesives and the effect of adhesive curing. The low curing heat of ICAs in general, are one of their main assets, and are widely used as an interconnect in heat sensitive electronics. The curing of the adhesive takes place at $<150^{\circ}$C and actually improves the contact between the filler particles, lowering the resistivity [9]. Typical applications could be in solar cells to replace the low temperature lead soldering that is used today [1, chap. 4.6.1].

The resistance of silver thin films have been investigated on different insulating substrates like glass and roughened substrates [10, 11]. Yet none have been conducted on individual silver films prepared on spherical polymer substrates with a wet chemical deposition, as the case is for the AgPS used in the ICAs. These measurements are done at bulk smaples of the adhesive, so how the silver coating thickness relates to the conductivity of bulk ICA is known [5]. Thicker silver films give a higher conductivity for volume concentrations of particles below 40%, above that, the conductivity is independent of film thickness. Investigations on single particles have however not been done, so it is not possible to separate singe particle properties from contact or bulk effects. The key to create a good foundation for further development of ICAs with AgPS is to improve the performance of single AgPS.

Conductive adhesives provide a way of connecting electrical circuits without using solder. By reducing the amount of precious metals in conductive adhesives, the cost goes down, and it will be competitive with normal soldering where there is a special need for low heat, more durable mechanical properties or where toxic metals like lead is not allowed. Applying AgPS as the conductive fillers in ECA, is a novel application. It is therefore essential to develop procedures to find a good way to characterise the electrical properties of the spheres to

further the development and commercialisation of metal containing ECAs.

This project aims to develop and test a method for accurate measurernts of electrical properties in spherical thin films on micron sized metal-coated polymer spheres, without imposeing a large mechanical deformation. Currently, methods for conducting electrical measurements on micron sized spherical thin films are lacking. Such a method should be accurate enough to show that different films (e.g. thickness, composition, coverage) will give different electrical properties. To achieve this, a four-wire measuring environment and equipment are optimised by changing different parameters. The effectiveness of the method will be demonstrated in a study of the resistance in metal-coated polymer spheres (MPS) of silver with different film thicknesses.

This master's study report explains the experimental method and some simulation basics in Chapter 3 before the results from the experimental method are presented in Chapter 4. Though some of the simulations are introduced already in Chapter 4, will most of the simulation be presented in Chapter 5. The following discussion and conclusion are in Chapter 6 and 7 respectively. Then finally, he outlook for further work presented in Chapter 8. But first, an introdution to the theory in Chapter 2.

2 THEORY

The theory chapter seeks to give a theoretical introduction to the instruments and methods employed in the experimental investigations and models. The first section will give an introduction to the charged particle (electron or ion) as a probe and its interactions with the target. The working principles and properties of the Focused Ion Beam (FIB) and the Scanning Electron Microscope (SEM) are given in Section 2.2. The working principles of the Atomic Force Microscope (AFM) used to investigate the AgPS surfaces, are introduced in Section 2.3. In Section 2.4, the specifications of the micromanipulators used for probing is given, before the electrical measurements are explained in Section 2.5. In the end, the principles of the modeling software used are described.

2.1 CHARGED PARTICLE INTERACTION

When employing charged particles in a focused beam to get information about the sample, the interaction between the particle and sample is very important. Contrary to the light microscope, where sufficient light reflected/transmitted is the main worry, a charged particle probe causes a lot of reactions when hitting a sample. Whether it is charged electrons or ions that creates the probe, the collision with other matter will cause emittance of new particles and possible backscattering and implantation. The result of the collision depends on the properties of the charged particles like mass, energy and charge. Different particle properties do also favor different information to be gathered from the interaction like topology, thickness, element, crystal structure etc.[12, 13, chap. 2]. High energy interactions can also sputter matter away or deposit material from precursors. In this study, a dual beam FIB-SEM is used which combine an electron column emitting electrons and a gallium (Ga) source producing gallium ions, Ga^+. As will be explained below, the different particles react with the target in distinctive ways.

2.1.1 *Electrons*

Electrons are very small and light particles. When a focused and directed electron beam hits a sample, the small size and high energy of the electron makes it possible to penetrate microns into the surface before it looses all of its energy. The energy is lost through a series of collisions with the sample matter in a restricted area called the sample's *interaction volume*, defined as the volume within 95% of the primary electrons are brought to rest, see blue area of Figure 2.1(a). From the same figure, some of the main interaction signals from these collisions are visualized [12, chap. 2.7.5].

The secondary electrons (SE) are the electrons that escape from the sample with energies below 50 eV. They are generated from both the electrons from the incident beam (primary electrons) and from the backscattered electrons (explained below). The former are by far the most numerous, and the number of emitted SE per primary electron (*yield*) can be higher than 1. They are therefore abundant and the most commonly used signal in SEM (see Section 2.2.2). As illustrated in Figure 2.1(a), the SE created from the primary electrons have only enough energy to escape from the topmost layer of the sample, originating from an area a little larger than the incident beam. This gives the SE the smallest sampling volume, thus having a better spatial resolution than the other signals [12, chap. 5.2].

The backscattered electrons (BSE) are created if the primary electrons are scattered out from the sample before they have lost all their energy. They are not as abundant as SE electrons, but they tend to have higher energies [12, chap. 2.8.2]. The yield of the BSE increase with increasing atom number (Z), and this is utilized to obtain a compositional contrast [12, chap. 5.2]. The BSE are also the cause of an effect called *electron channeling*. This effect is dependent on the crystal orientation with respect to the incident beam [12, chap 5.8.1]. The BSE coefficient, how much BSEs are reflected from the sample, is large if the crystallographic plane is perpendicular to the beam causing the electrons to bounce back rather than travel far into the sample giving a high signal. If the beam is parallel to the crystal planes, most of the electrons will travel deeper inside the sample, thus a low BSE coefficient and signal. This is a weak contrast compared to the Z-contrast.

2.1.2 *Ions*

The Ga ion is 130 000 times heavier and 20 000 larger than the electron. Thus the penetration depth of the ions are usually in the range of a few nm due to the high probability of colliding with nuclei in

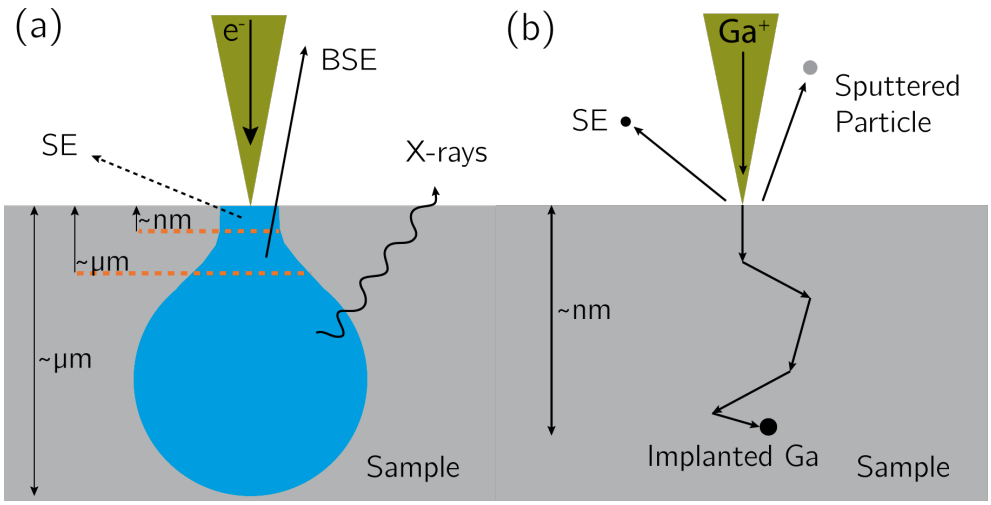

Figure 2.1: The interaction between charged particles and the sample. Electrons, (a), have a large interaction volume, penetrating deep into the sample, emitting signals from all depths: Secondary electrons (SE), Backscattered electrons (BSE) and x-rays. The Ga-ions in (b), have a much smaller penetration depth, creating signals only from the topmost layers. (a) is adapted from [12, fig. 5.6, chap. 5.2] and (b) is from [13, fig. 2-1, chap. 2.1].

the target [14, chap. 1.2]. The high energy impact when a Ga-ion collides with a sample, knocks out atoms that may be ionized, called secondary ions (SI). When a target atom is knocked from its position, it can contribute to the *collision cascade* [13, chap. 2.2.1]. The collision cascade can best be described as a moving sea of particles within a solid. The cascade emits SE before the ion moves into rest in the sample. In addition, a particle from the solid can be sputtered away if sufficient momentum is transferred from the collision cascade to the surface, see Figure 2.1(b). Another result of the hard impact from the Ga-ions, is that the affected region of the sample turns amorphous.

2.2 THE DUALBEAM FIB/SEM

The dual-beam incorporates both a Focused Ion Beam (FIB) column and a Scanning Electron Microscope (SEM) column in a single system. The configuration used in this project is that of the *FEI Helios NanoLab DualBeam FIB* where the ion beam column is tilted in an angle of 52° from the vertical electron column [13, chap. 12.2]. The electron beam is used for non-destructive navigation and imaging of the sample, while the ion beam is used as a manipulation tool for milling the flat

punch probes, see Section 3.3. In the following sections, the working principles of the FIB and SEM are explained.

2.2.1 *FIB*

The FIB system is designed to efficiently utilizing the ion-sample interactions introduced in Section 2.1.2. Gallium (Ga^+) ions are usually employed in FIB systems because of their low melting point, intermediate mass and size and low volatility at the melting point [14, chap 1.1.3]. The FIB Ga source is a liquid ion metal source (LIMS). LIMS emitters are point-like ion sources with a high intrinsic brightness [15, chap. 3.2.1], having tunable energy and intensity proved ideal for FIB applications. The source, together with a combination of apertures and electrostatic lenses, can under the right conditions give a resolution down to 10 nm [15, chap. 3.3.1]. The ion beam hits the sample in a evacuated chamber, the sample being on a stage that can move in the x-, y- and z-directions together with tilt and rotation. But the vacuum chamber is not large enough for all this types of movement with the micromanipulators inside, Section 2.4.

2.2.1.1 *Milling*

The FIB can be used to mill the target by the means of physical sputtering. The sputtering is initiated by elastic collisions between the ion and nuclei of sample atoms, leading to a collision cascade, as mentioned in Section 2.1.2. Enough momentum transferred to a surface nucleus causes the particle to sputter away from the target [13, chap. 2.1]. The FIB uses this effect to mill the target, but the milling performance is highly dependent on the channeling effect:

Channeling (not to be confused with electron channeling in Section 2.1.1) is a process where ions penetrate greater distances along low index directions (i.e [100] or [111]) compared to non channeling directions or amorphous materials. The channeling causes a contrast between materials and is dependent on the interatomic planar distances and the atomic density. As a consequence, close packed crystal structures with higher atomic densities like copper, gold, and tungsten have a much more significant channeling effect than materials with lower atomic densities as silicon [13, chap 2.4.3]. The channeling contrast have also a great effect on the sputtering yield. The sputtering rate is significantly slower for high channeling directions, but at the same time resolution is better and redeposition artifacts are less prominent. The trenches caused by channeling can partly be overcome by first depositing a protective metal layer of for instance chromium.

The milling next to this protective layer will not result in a channeled topography after sufficient milling time.

2.2.2 *SEM*

The Scanning Electron Microscope (SEM) scans a beam of electrons over the sample with voltages from 3-30 kV. The electron beam is produced with a Field Emission Gun (FEG) which use extremely high electric fields to achieve a high source brightness (see Section 2.2.2.1). The FEG source is followed by a condenser and objective lens gathering and demagnifying the electron beam. Spherical aberration is minimized by adjusting the aperture placed in the column before the beam hits the sample. The lenses in the SEM are electromagnetic contrary to the electrostatic lenses used in the FIB ion column. The most utilized signals generated from the impact with the sample, are shown in Figure 2.1(a). But in general, the SE are the most used signals detected with a Everhart-Thornley detector [12, chap. 5.2].

2.2.2.1 *Resolution*

The magnification in SEM is governed by the microscope's ability to focus the beam. When the raster made on the specimen by the electron beam is smaller than the raster on the display device, the sample image is magnified. A consequence of narrowing the probe diameter, is that the current I decreases as the condenser strength decreases. If the semi-angle of the the rays leaving the condenser is α_0, and the semi-angle of the rays entering the objective lens is α_1, the probe current can be described as equation 2.1 [12, chap. 5.3]:

$$I_1 = I_0 \times (\frac{\alpha_1}{\alpha_0})^2 \tag{2.1}$$

The direct result being that by increasing the magnification, a weaker current is achieved which ultimately will cause the signal to be insufficient for imaging. This will also affect the resolution; a weak signal will cause a poor contrast for both topography and composition. At low currents signal noise and low vacuum effects become more influential, lowering the resolution. A FEG SEM can overcome most of these artifacts down to a resolution of ~1 nm thanks to its high brightness [12, chap. 5.3.3]. However, the low vacuum in the DualBeam FIB, makes such resolutions hard to obtain.

2.2.2.2 *Imaging and Artifacts*

To explain how the image is created, the raster has to be addressed again. The beam moves over the sample in a known pattern. The signal from each step corresponding to one pixel in the monitored image. In the FIB-SEM setup the Everhart-Thornley detector has a free path to the sample. That means that not only SE will be picked up, but also some BSE directly in the path towards the detector [16, chap. 29.8]. The BSE noise could be effects from both Z-contrast and channeling effects.

There are other factors that can also affect the SEM imaging, here are some artifacts [12, chap. 5.10]:

CHARGING is the phenomenon of electrons that accumulate in the poorly conducting specimen. One of the major drawbacks of SEM is that the sample has to be electrically conducting to avoid charging. A sample not connected to earth will become increasingly negatively charged until incoming primary electrons are repelled and deviated from their normal path. This causes a bright and distorted image. The high electrostatic charge can cause movement in parts of the sample leading to a distorted image as well.

BLEEDING PIXELS is an artifact that appears at high magnifications. It is caused by the signal from the SE that bleed into nearby pixels because of the interaction volume being larger than the designated pixel. The result being a more blurry image.

VIBRATION and THERMAL DRIFT can cause jumps and glitches in the raster, degrading the image quality.

2.3 AFM

The Atomic Force Microscope (AFM) differs from the FIB and SEM in the way it interacts with the sample. The AFM interacts with or touches the surface mechanically with a tip, by detecting near-field forces between the tip and the sample. When the tip is moved in a raster over the sample, the resulting data map can be used to get information about the topography, mechanical properties, phase etc. AFM is not dependent on vacuum and electrically conductive samples [17, chap. 5.3].

2.3.1 *Working Principles*

The AFM works by scanning a thin tip over a surface in a raster. On the rear side of the tip cantilever, a laser beam is deflected hitting photo diodes arranged in four quadrants, Figure 2.2. The movement is compensated by adjusting the sample stage through a feedback circuit. This information is interpreted in different ways depending on the cantilever and feedback setup.

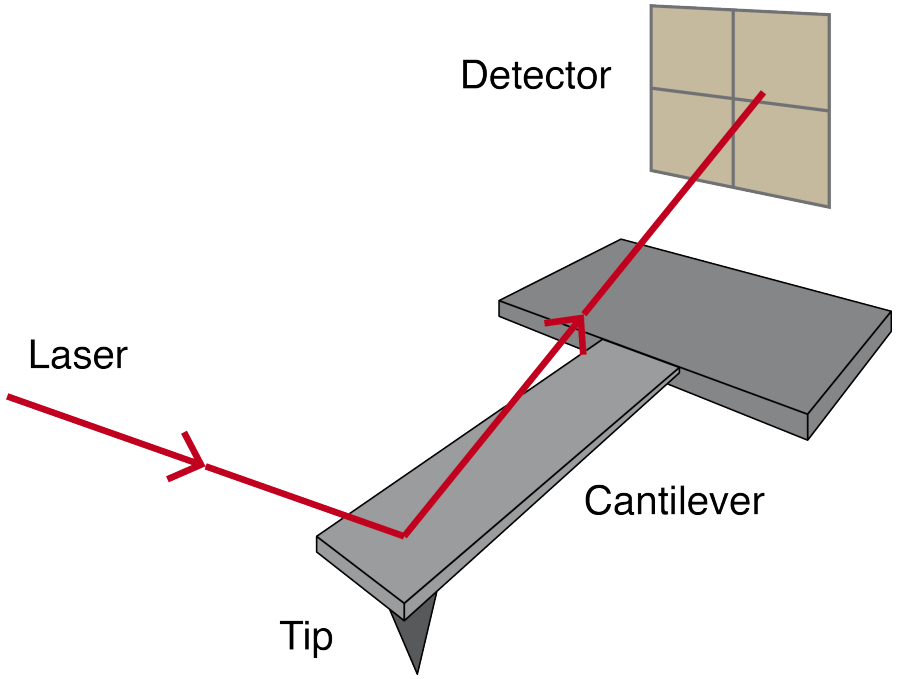

Figure 2.2: The AFM detector consists of four-quadrant photodiodes. When the cantilever is moved by forces exerted on the tip, the laser pointing at the cantilever head is reflected upon the detector. Deflections of the cantilever result in a different reflection registered at the detector.

2.3.2 *Imaging*

The instrument the *AFM Veeco multimode V* from BRUKER was used for all AFM instigations. This instrument has installed a special detection mode called PeakForce Quantitative Nanomechanical Mapping (QNM). The PeakForce QNM is a dynamic tapping mode, but differs from the conventional tapping mode where the cantilever is actuated as an harmonic oscillator with a set frequency. In the conventional mode, the topography data can be found by recording how the varying force field on the tip changes the amplitude of the oscillating tip [17, chap 5.3.3].

One of the simplest measurements to do with an AFM, is to do a single point measurement by lowering the tip into the surface and measure the force exerted on the tip as a function of the tip-sample distance. This single point measurement creates a *force curve*. In PeakForce QNM tapping, the maximum force on the tip is controlled during the acquisition of the force curve [18], rather than the oscillating amplitude in normal tapping mode. This force approach makes the AFM easy to use, non-destructive to tip and sample, and gives a high resolution mapping of the samples properties both topological and compositional.

2.3.3 *Resolution*

There is not just the operation mode that sets the resolution and quality of the image, other parameters do also have an impact. The tip radius and shape greatly affects the resolution. The tip geometry may alter the lateral dimensions as seen in Figure 2.3. The tip can also be damaged or uneven at the side slopes, which can also affect the representation of the sample.

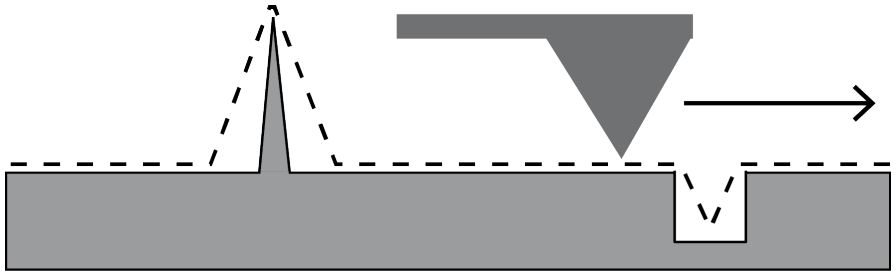

Figure 2.3: The size of the tip has an effect on the size of the detected topological features. A large tip will cause the peaks to appear larger than what they are and trenches will appear smaller.

Among the parameters that can have a large influence on the resulting image, is the gain and the peak force amplitude. The gain parameter controls in which degree the sample stage reacts to a change in the signal. A good result is dependent on precise tuning of this parameter. The peak force amplitude controls the oscillation and the force the tip hits the sample with. This is important to tune right in order to avoid tip and sample damage. The PeakForce QNM mode have a automatic gain and peakforce mode which makes it very easy to obtain good results [18]. That being said, typical AFM artifacts like spikes and blurry areas caused by the tip failing to follow the surface can still be an issue. These artifacts are a result of a sudden change in the surface topography that the feedback loop does not manage to adjust for.

2.3.4 *Surface Properties*

The AFM gathers detailed information about the surface topology. In order to compare surface topology obtained by the AFM data, a set of parameters is used to describe the topology numerically. The Finite Element (FEM) analysis, Section 2.6, uses two of these parameters, see Figure 2.4, which are also explained below.

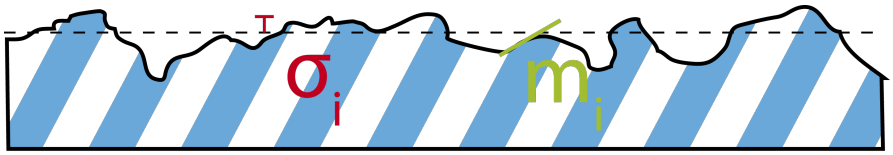

Figure 2.4: A surface with the mean image data plane marked with the stippled line. The height deviations from the mean (red) and the surface slope (green).

The root mean square is the square root of the arithmetic mean of the squares of the values. This method is employed when the height deviations, Z_i, taken from the mean image data-plane of an AFM dataset to calculate the Root Mean Square (RMS) surface roughness, R_q, in Equation 2.2[19]. The R_q corresponds to the asperities average height input, σ_i, in the FEM analysis for electrical contacts, see Section 2.6.2.

$$R_q = \sqrt{\frac{\sum Z_i^2}{N}} \tag{2.2}$$

The RMS gradient of the surface, S_{dq}, comprising the surface and evaluated over all directions, is given in Equation 2.3. This is given in degrees, but can easily be transferred to the RMS surface slope, $m_i = \tan(S_{dq})$, in the electrical contact model mentioned above.

$$S_{dq} = \sqrt{\frac{1}{A}\int_0^{L_x}\int_0^{L_y}\left(\left(\frac{\partial}{\partial x}Z(x,y)\right)^2 + \left(\frac{\partial}{\partial y}Z(x,y)\right)^2\right) dy\,dx} \tag{2.3}$$

2.4 MICROMANIPULATORS

The micromanipulators used in this project were delivered by IMINA TECHNOLOGIES. The miBot^{TM} BT-11-VP is placed on and connected to a miBase BS-43-VP. The miBot is a mobile mini robot which can be positioned and manipulated at micro- and nanoscale. Figure 2.5 show

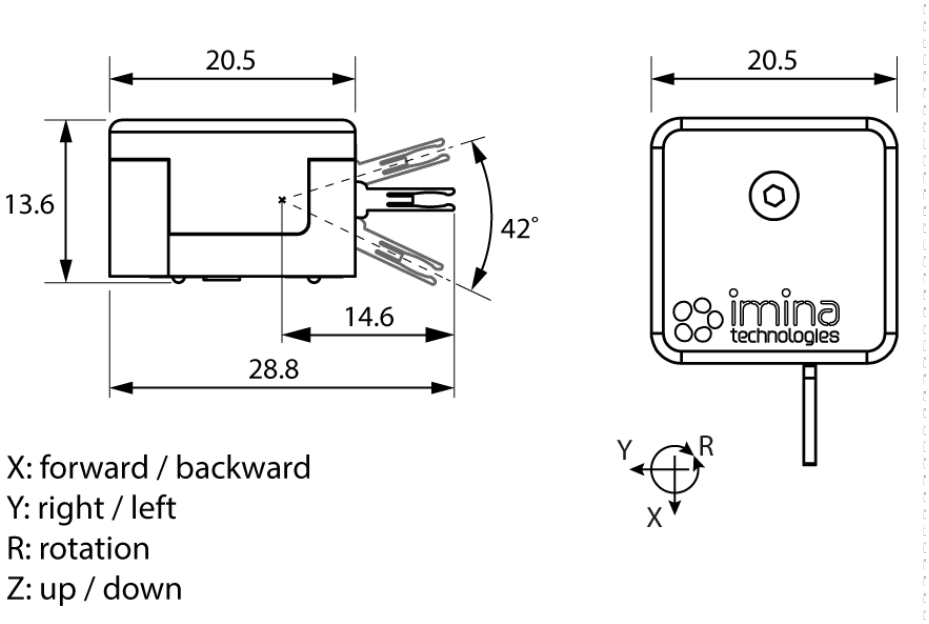

Figure 2.5: A schematic of the miBot^{TM} BT-11-VP, the measurements are in mm. The manipulator can be moved with four different degrees of freedom. The schematic is taken from the technical specification sheet[1].

the outline of the miBot and its direction of movement. The miBot has a maximum pushing force of 0.3 N and a holding force of 0.2 in x- and y-direction, but no force control exist. The other ranges and limitations given from the manufacturer are given in Table 2.1[1]. The probe stepping have a transition from mechanically driven to a piezo actuator for the smallest stepping sizes.

Table 2.1: Overview over some key properties of the miBot^{TM} BT-11-VP.

Stepping resolution	X	60 nm
	Y	40 nm
	Z	100 nm
Max speed	X	2.5 mm s^{-1}
	Y	2.5 mm s^{-1}
	Z	150 mrad s^{-1}
Probing signal	Voltage	$\pm$100 V
	Current	100 fA-100 mA
	Resistance	typ. 3.5 Ω

The probes are reported to be very precise in its movements, the limiting factor mostly being the tip size of the probe [20]. The resistance of 3.5 Ω is from the probe tip to where the flex cable is connected to the stage. The connections through the miBase stage, the cables and vacuum sealed connectors have a resistance of ~2.6 Ω. Obviously do these numbers change from installation to installation, so these numbers are only for guidance. An experimental resistance test for the employed system is done in Section 4.3.1.

2.5 ELECTRICAL MEASUREMENTS

To get an understanding of what electrical properties that are measured, some basic equations explaining how electricity is understood today and what assumptions that are usually made are presented here. The calculations used in this project assumes that the measured silver thin film is homogeneous and isotropic. Beginning with the resistivity, ρ [Ωm], this relates the applied electric field to the current density:

$$E \equiv \rho J \tag{2.4}$$

E is the electric field [V/m] and J is the current density [Am^{-2}]. Equation 2.4 is one form of Ohm's law [21].

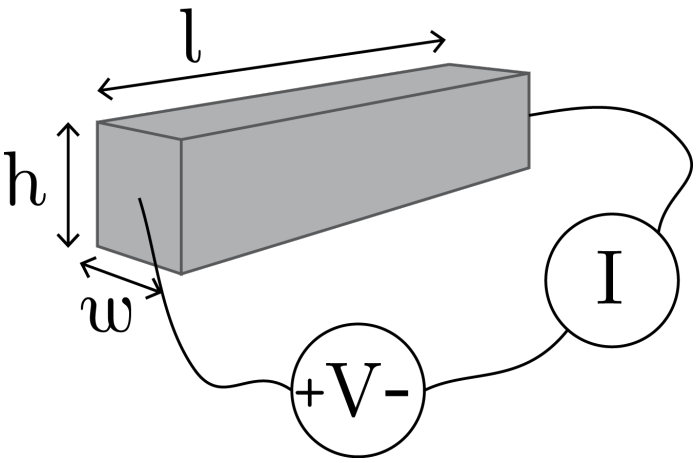

Figure 2.6: A simple outline of a two-wire measurement. The voltage source V and ammeter (to measure the current I) are coupled in series with the object to be measured.

1 Numbers taken from the technical specifications sheet available at `http://imina.ch/`

Considering the bar geometry in Figure 2.6, the electric field E is expressed by the voltage V divided by the distance l over which the voltage is applied, Equation 2.5.

$$E \equiv \frac{V}{l} \tag{2.5}$$

The current density J through the bar in Figure 2.6 is the current I divided by the cross-section in which the current flows.

$$J \equiv \frac{I}{A} \tag{2.6}$$

A in Equation 2.6 is equal to the height h times the width w. When Equation 2.4, 2.5 and 2.6 is combined and rearranged, an expression with only current, voltage and geometrical expressions is achieved:

$$V = \frac{I\rho l}{A} \tag{2.7}$$

Finally, from Equation 2.7 the resistance, which is sought after in this project, can be defined:

$$R = \rho\frac{l}{A} \tag{2.8}$$

As a reminder is ρ the resistivity, l the length of which the current travels, and A the cross section the current has to travel through. Combining Equation 2.7 and 2.8 the most familiar form of Ohm's law is revealed:

$$I = \frac{V}{R} \tag{2.9}$$

I is the current in ampere [A], V is the voltage [V] and R is the resistance in ohms [Ω].

2.5.1 *Two-wire Measurements*

The resistance of a material can be obtained by a method called the two-wire probing technique. As the name implies, two wires are attached to each side of the geometry to be measured. Then a voltage source applies a voltage V across the the geometry, causing a current I to flow through [21]. In other words, the technique measures the

current flow at a set voltage (or the voltage at a set current). In this technique all the components are coupled in series (see Figure 2.6), and the resistance that is calculated from the measured current will thus be the sum of all the resistances in the circuit, including the ammeter and the wires. When sufficient contact between the probes and AgPS is achieved, an Current-Voltage (I-V) sweep over the particle displays a linear relation between current and potential, Equation 2.9. The resistance is the result of finding the slope of this linear region:

$$R = \frac{\Delta V}{\Delta I} \tag{2.10}$$

The slope in Equation 2.10 is found by taking a least mean square linear fit[1] to the measured I-V curve, this process is automated in a *Matlab 2014b*[2] script, Appendix B.

Though simple, the two point measuring technique is not always reliable [21]. For example if the resistivity of the sample is low, the resistance contribution from the equipment itself, between contact probes and the material, and in the wires will be significant. Consequently, the measured resistance is always higher than the sample resistance, although this difference is negligible for high-resistance samples. Knowing the voltage drop across the different components in the circuit will help, but the contact resistance is a challenge.

To have good electric contact between probe and film, is always a challenge in resistance measurements. Ideally the surface should be flat, clean and without oxides [21]. The AgPSs are spherical and probably have a thin oxide layer of Ag_2O. The silver film roughness also gives rise to an increasing porosity compared to bulk. At low loads typical for the conducted measurements, such a rough surface gives less reliable contacts [22, chap. 8.3.3].

High electric loads and low voltage in small areas can cause heat to develop, *Joule heating*. In metals, when the temperature of the material is increased, so does the resistivity. A way to check for Joule heating is to make sure the measured resistance does not drift more than 10% in a few minutes [21].

2.5.2 *Four-wire Measurements*

The four-wire measurement employs four probes in order to measure the resistance in stead of two. A seen in Figure 2.7 the outer wire is

1 See Matlab documentation for *polyfit*: `http://se.mathworks.com/help/matlab/ref/polyfit.html`

2 See documentation for Matlab at `http://matlab.com`.

connected to the side of the bar and a voltage is applied over the bar, resulting in a current I through the sample. The inner circuit picks up the voltage drop over the length of the bar spanned in between, l' [21].

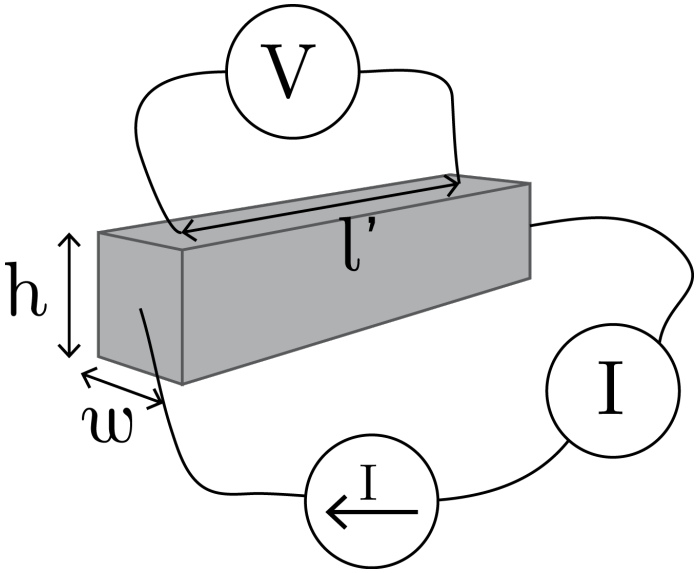

Figure 2.7: Four wires are attached to the bar in the four-wire method. A voltage source forces a current thorugh the bar, measured by a separate ammeter. A separate circuit with a voltmeter measures the potential across the middle of the bar.

The output of the four-wire measurement is as for the two-wire measurement, an I-V curve. The resistance is found by the same procedure, Equation 2.10, but the method is much more accurate. The separation of the current and voltage measuring circuit, makes it possible to measure the resistance without any influence of the contact resistance at the probe contacts. This is because extremely little current flows through the inner pair of contacts connecting the voltmeter, thus no voltage drop occurs at the voltage probe contacts [23].

When doing four-wire measurements, there are some additional properties to take into account [21]: Large sized voltage probes or if the probes are placed too close to each other, could reduce the accuracy of the resistance measurement. Ideally the voltage contacts should be made small or as thin as possible, and the distance between them should be much larger than the sample thickness. The four contacts should be completely independent of each other. This can be a challenge when each I- and V-probe pair should be as close as possible to obtain the most accurate results.

The current can choose different paths when traveling through a thin film. For a four-wire measurement at a microscopic scale on a flat

sample, the current will not be able to penetrate deep into the sample as the distance between the I-probes is too small [23]. Thus the surface layers are contributing most to the measured resistance. Increasing the probe distances will allow more of the current to penetrate deeper into the film, allowing more of the bulk to contribute to the measured resistance. How these effects would translate to a spherical thin film, has yet to be investigated.

2.5.3 *Resistance Considerations*

For thin films of metals like silver, the resistivity is dependent on multiple factors. A thin film will approach the bulk resistivity of 1.59 $\mu\Omega$ cm, if the film is above a certain thickness, has a smooth surface, large grain size and a low reflectivity grain boundary [24]. For silver films with a thickness below the Electon Mean Free Path (EMFP), which for silver is 52 nm at RT, the resistivity increases almost linearly. The EMFP is the mean distance an electron travels in a bulk material before colliding with the lattice. It has been hard to separate the EMFP from the other resistivity influencing factors mentioned earlier, but it is safe to assume that the size effect also contributes. The EMFP and size effects can first be neglected for films thicker than 100 nm [11]. None of these experiments are done with spherical silver films or with chemically deposited silver, as sputter coating on a flat substrate is the norm.

Since the silver thin films to be measured are thicker than 80 Å, they obey Ohm's law Equation 2.9, which means that it is a linear relation between the potential (V), and current (I) [11]. For the contact between the probes and the AgPS film, Equation 2.11, Holm's model for contact resistance, R_c,between two materials can be used [22, chap. 1.2.1]. This applies if the contact consists mainly of two materials and the contact area is circular, however the real contact area are far from this ideal representation (see Section 2.5.1). ρ_1 and ρ_2 is the resistivity for the two materials respectively, and a is the contact area radius.

$$R_c = \frac{\rho_1 + \rho_2}{4a} \tag{2.11}$$

A quick calculation of the contact resistance using the bulk resistivity of silver and tungsten (W), $\rho_W = 5.28 \times 10^{-8}\,\Omega$m [25], with a contact radius of 1 μm, can be done for reference: According to Equation 2.11, this gives a resistance of 0.034 Ω. This resistance is negligible for the two-wire measurements, as the measured resistance is much higher. The four-wire measurements, omits the contact resistance by nature of the setup.

2.6 COMSOL MULTIPHYSICS

COMSOL Multiphysics is a Finite Element (FEM), Partial Differential Equation (PDE) simulation software that can be used to mimic physics in real-world applications. By combining multiple scientific models of different physics in an advanced numerical solver, the results from the COMSOL Multiphysics models is as good as the materials coefficients and other assumptions employed when building the model [26]. COMSOL's strength lays in the ability to combine different physical regimes in order to model coupled physics phenomena, but in this simple analysis, only the *AC/DC electrical currents* will be used.

2.6.1 *The Mesh*

Many physical phenomena in science can be described by in terms of PDEs. Since it in general is impossible to solve these equations for arbitrary shapes, the FEM is applied. The FEM can solve these PDE approximately by dividing the model body into finite elements connected by nodes. This is called the finite element mesh [27]. The mesh size can be tuned to get a more exact answer. Smaller elements (also called domains) give a more thorough simulation, but do also demand more computational power. Another way of obtaining a more exact answer is by increasing the nodes that connect the domains in the mesh. That being said, neither a finer mesh nor more nodes does not automatically give a result closer to reality, as the assumptions made when building the model often is the limiting factor.

The mesh size is a trade off between getting high precision results thus a long computation time, and a shorter computation time with results of poorer precision [27]. In COMSOL Multiphysics this can be solved by tailoring the mesh so that the most critical areas with high gradients, have a fine mesh and the other parts a rougher mesh. Thus the areas where the I-probes are in contact with the silver coating, should have a fine mesh together with where the V-probes measure the potential.

In COMSOL Multiphysics the mesh is usually constructed by tetrahedral domains. The domains are created automatically based on the user inputs and constrains: The maximum and minimum size of the tetrahedrons. The maximum element growth, which specifies how fast a fine masked area of tetrahedrons can grow into the rougher surrounding size. The curvature factor and resolution of narrow regions which sets the masking in curved areas and narrow regions respectively.

2.6.2 *The electric Currents Interface*

To model the experimental resistance measurements, the electric currents interface in the AC/DC module was used to simulate the physics. This is based on the current conservation node that adds the continuity equation for the electric potential, $\mathbf{E} = -\nabla V$, and implements the electrical properties from the materials in the model[3].

The contact between the probes and the silver coating is the most important feature in the model. To make this work, an electrical contact is defined between the probes and coating based on the Cooper-Mikic-Yovanovich (CMY) correlation to find the joint conductance at two contacting surfaces[28]. The electrical contact defines correlations for the contact conductance, h_c, at the interface of to bodies in contact, Figure 2.8.

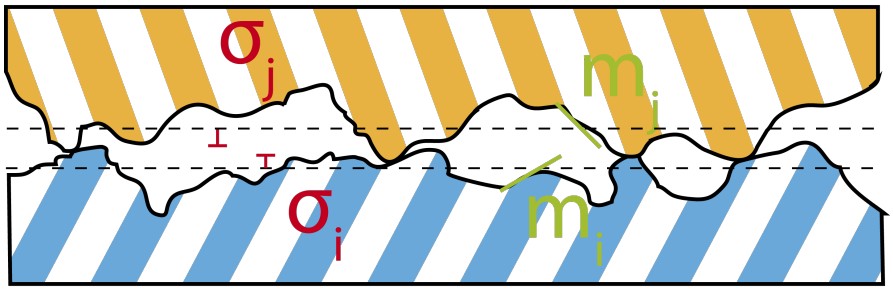

Figure 2.8: Two surfaces brought in contact to transfer current. The surface average height and slope have been found in advance, Section 2.3.4, and are combined by the taking the root mean square (RMS), Equation 2.12.

The topological properties of both the contact surfaces are combined by the taking the RMS, as seen in Equation 2.12. Regarding this specific experiment, only the surface values from the silver coating are found and employed in the model. The FIB milled tungsten probes are thought to have a much finer surface, and they are ignored here.

$$\begin{aligned} \sigma_{RMS} &= \sqrt{\sigma_i^2 + \sigma_j^2} \\ m_{RMS} &= \sqrt{m_i^2 + m_j^2} \end{aligned} \tag{2.12}$$

The CMY correlation is formulated by using a model that assumes plastic deformation of isotropic rough surfaces. It is however, impor-

3 Information based on the COMSOL Multiphysics documentation concerning the AC/DC module.

tant to note that this model has no memory. So the plastic deformation of the surface asperities are neither computed nor stored: A load applied twice will result in identical electrical contact. The contact conductance h_c, is then CMY defined as Equation 2.13 [29]:

$$h_c = 1.25\sigma_{contact}\frac{m_{RMS}}{\sigma_{RMS}}\left(\frac{p}{H_c}\right)^{0.95} \tag{2.13}$$

The RMS surface asperities m_{RMS} and σ_{RMS}, are from gathered topographic data of the contacting surfaces. The p is the contact pressure the probes are indented with. H_c is the microhardness of the softer material, in this case silver, and $\sigma_{contact}$ is the harmonic mean of the contacting surface conductivities, Equation 2.14:

$$\sigma_{contact} = \frac{2\sigma_i\sigma_j}{\sigma_i + \sigma_j} \tag{2.14}$$

3 EXPERIMENTAL

The main objective of this master project has been to develop a four-wire measurement method that enables the measurement of the resistance of a single silver coated polymer sphere (AgPS). The AgPSs are introduced in Section 3.1 followed by a sample and probe preparation section. The resistance measurement setup is explained in Section 3.4 both with respect to the simple two-wire and the more complicated four-wire measurements. The resistance simulations are performed in COMSOL Multiphysics are described in Section 3.5. The last section explains the procedure for the AFM topographic investigations.

3.1 THE SILVER-COATED POLYMER SPHERES

The AgPSs investigated in this report are supplied by Mosaic Solutions AS; a daughter company of Conpart AS. They are made from monodisperse polymer spheres coated with silver by a chemical deposition reaction. For the measurements in this report, monodisperse polymer particles made of PMMA with low crosslinking density and a diameter of 30 μm were used. They were silver coated with four different thicknesses. According to the manufacturer, one batch should have a silver-coating of 60 nm, 100 nm, 150 nm, and 270 nm, from now on called 60Ag, 100Ag, 150Ag, and 270Ag respectively, see Figure 3.1. The coating thickness was estimated by the manufacturers from the amount of silver precursors consumed in the coating process. The spheres were produced following the same procedure, and have the same polymer core. The thickness (and thickness related effects) of the silver-coating should therefore be the only parameter differentiating these AgPSs.

3.2 SAMPLE PREPARATION

The samples were both prepared so they can be viewed and manipulated inside a SEM as well as characterized by an AFM. The prepared samples should therefore fulfill the following requirements: Neither

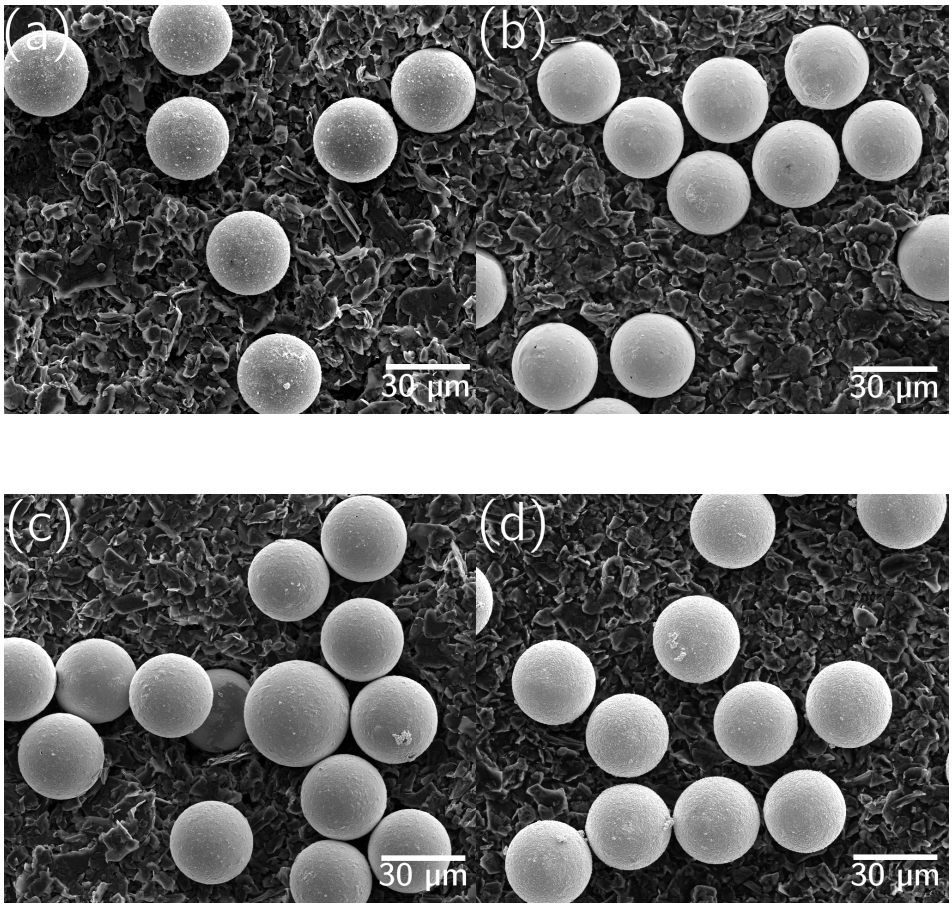

Figure 3.1: Micrographs of all the different AgPSs investigated in this project. (a) shows the 60 nm Ag coating, 60Ag and (b), (c), and (d) show the 100Ag, 150Ag, and 270Ag respectively.

the substrate nor the substrate adhesive should be insulating. In addition the adhesive must offer a good support for the AgPSs when handled with the probes or the AFM.

The substrates used for all the measurements were 1 cm quadratic pieces cut of from a 0.65 mm thick silicon (Si) wafer. Conductive Carbon Cement (CC) (LEIT-C) from AGAR SCIENTIFIC, UK was used as an adhesive for all the samples.

3.2.1 *Preparation Method*

A previously encountered problem has been that the AgPSs have not been sufficiently attached to the substrate. To ensure good adhesion and an overall adequate sample quality, the following method for preparing the samples was developed:

1. The LEIT-C CC is first thinned with the LEIT-C thinner to ease the distribution of the cement on the substrate, as well as making it easier for the AgPS to be submerged in the cement.
2. A thin and even layer of CC is distributed over the Si substrate with a sharp blade.
3. A small pinch of dry AgPSs are sprinkled over the CC, with the aim to have as few agglomerates as possible.
4. The Carbon Cement is allowed to dry for 30 seconds.
5. A thin and light plastic tube with a diameter of 3.25 mm is gently rolled over the sample to force the particles down into the cement.
6. The sample is ready after 30 min curing in room temperature.

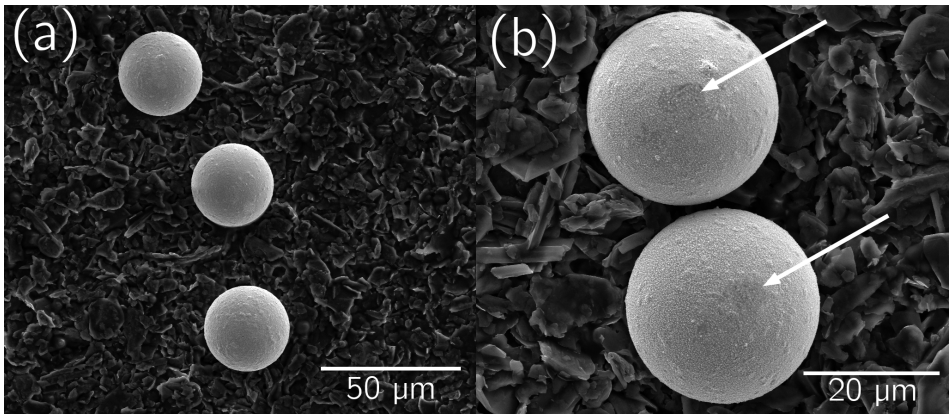

Figure 3.2: Two micrographs of the 100Ag. (a) shows lightly attached spheres, without any visible damage. Darker spots as a result of the mechanical rolling, are marked with white arrows in (b). The spheres are at the same time more submerged in the CC, having a better adhesion to the substrate.

After these preparation steps, the prepared sample was inspected in an optical microscope to ensure that there are sufficient spheres present and that the spheres were not to agglomerated. Further inspection with a SEM revealed that some of the sphere surfaces took a small damage from step 5 in the sample preparation, Figure 3.2. It was therefore a trade off between excellent substrate adhesion and a small mechanically induced damage of the silver coating. Since measurements proved to be possible without totally fixed AgPSs, a better adhesion was sacrificed in exchange for visually undamaged particles.

3.2.2 *Stage Preparation*

The prepared sample was fixed onto one of two different stages dependent on the characterization instrument to be used. If the sample was to be inspected by an AFM, a small magnetic disc was glued onto the back of the substrate. If the sample was to be characterized in the FIB/SEM with the micro manipulators (miBots), the sample was attached with carbon tape to a designated FIB stub. The two different stages can easily be detached after use, enabling the same sample to be used with both instruments.

3.3 PROBE PREPARATION

Each AgPS is measured individually. To ensure a good electrical contact between the silver coating and the probes, operated by the micromanipulators, special polycrystalline tungsten (W) probes are prepared. The probes are supplied by IMINA TECHNOLOGIES and have a sharp tip with diameter ~0.5 µm. The tip was milled down with an ion beam in a *FEI Helios NanoLab DualBeam FIB* to ~2 µm diameter flat punch probe, Figure 3.3. An acceleration voltage of 10 kV was used with a current of 0.98 nA for the rough milling and 90 pA for the finish. From the calculations in Section 2.5.3, a contact area of ~2 µm is sufficient to ensure a steady supply of current and good voltage measuring conditions for both setup measurements (without taking silver coating roughness into account).

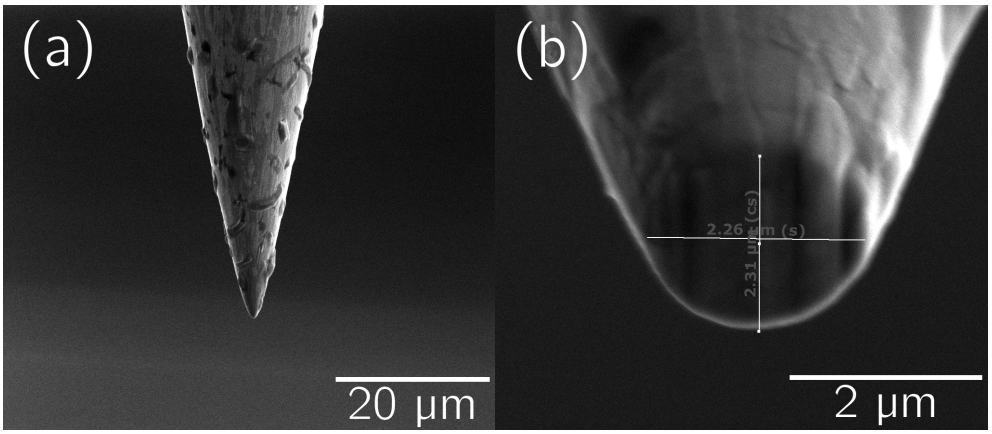

Figure 3.3: The unmodified probe as it is delivered from the manufacturer, (a). In (b) the same probe is milled down with the ion beam. The diameter of the probe tip is now 2.3 µm.

The probes were subjected to wear and tear. Both from the mechanical probing of the AgPSs and from the electrical measurements which could result in Silver (Ag) and Poly(methyl methacrylate) (PMMA) residues on the probe. More general handling of the probes do also contribute to wear of the probes; when they were disassembled for storage after use or when cleaned with an ethanol swab.

The probes also seem to be passivated, maybe with an oxide layer, after a 3-4 weeks without use. The probes can then be "activated" again by passing a high current through them. This method combined with ethanol swab cleaning, removed visual contamination and the probe behavior went back to normal.

During and in between measurements, the geometrical shape of the probes have sometimes had minor changes like bending and roughing of the tip. There have not been possible during measurements to determine whether this have resulted in changes in the data obtained or not.

3.4 RESISTANCE MEASUREMENTS SETUP

The resistance measurements were done with probes mounted on micromanipulators (miBots). They were coupled to a *Agilent B2909A Precision Source/measure Unit* multimeter. The multimeter data were recorded by a connected computer.

3.4.1 *Micromanipulators*

The micromanipulators were set up in a *FEI Helios Nanolab 600 Dual-Beam FIB* and they were used to do all the measurements. The set-up consists of four miBot™ BT-11-VP placed on a miBase BS-43-VP from IMINA TECHNOLOGIES[1]. The miBots were controlled through a graphical user interface on a connected computer. The navigation of each miBot was eased by a game pad controller that gives precise control over the movement in all possible directions. The system was operated inside the vacuum chamber of the above mentioned FEI FIB-SEM. The electron beam was used to observe the movements of the micromanipulators in situ. For the two-wire measurements, only two of the miBots were needed at the time, as for the four-wire measurements all four micromanipulators were in use, Figure 3.4.

From the way the miBots are designed, see Section 2.4, they may not always move precisely as commanded. Each probes characteristic movement must therefore be taken into account, especially in the pre-

1 http://www.imina.ch

cision placement cases. A typical example being that the probe moves slightly to the left upon descending. See Appendix A for more tips.

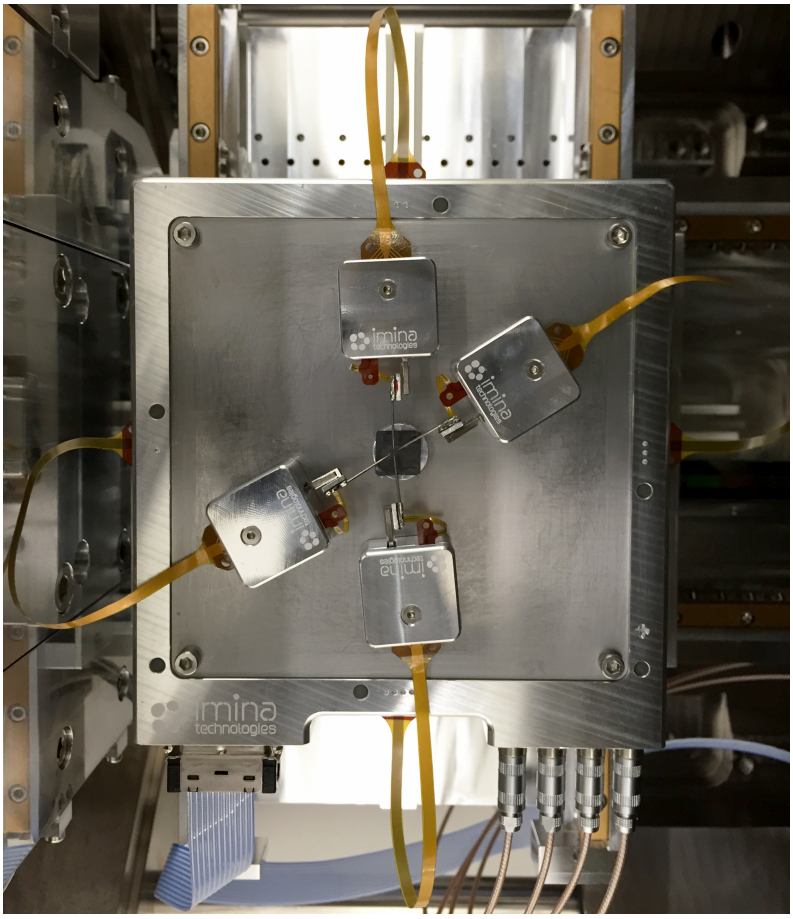

Figure 3.4: Overview of the setup of the miBots. The miBots are in a X-shape for the probes to be able to access two at the same side without interfering with another. The dark square in the middle is the substrate with the AgPSs fixed to the stage with carbon tape.

3.4.2 *Two-wire Measurements*

The resistance measurements were performed with probes mounted on micromanipulators (miBots). They were coupled to an *Agilent B2909A Precision Source/measure Unit* multimeter. The multimeter was coupled to a computer which could run I-V sweeps and obtain the resulting data from the multimeter. The obtained I-V curve from each sweep was immediately shown to evaluate the success of the measurement. The data from the I-V sweep, as well as a SEM picture of the probe-particle system were stored after each measurement.

Every particle was measured seven times consecutively. The probes were not moved between the first and last recorded measurement.

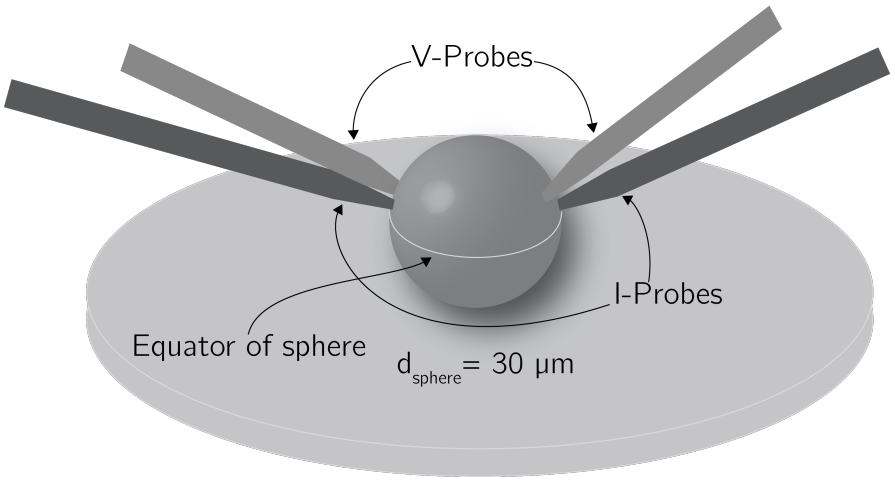

Figure 3.5: The tungsten probes are attempted to be placed like in this figure before each measurement. The I-probes slightly above the equator of the sphere and the V-probes in from the sides and slightly above in as close proximity as possible without short circuiting. The angle of the probes points downwards due to the elevated position of the probe holders on the miBots relative to the top of the substrate.

Some creep or unintended movement may occur, and this must be taken into account when analyzing the results. The probes were placed as seen in Figure 3.5, with the exception of the V-probes which were not present for the two wire measurements. The goal is to place the probes as close to the sphere equator as possible to have a common reference point from sphere to sphere.

The two-wire measurements on the AgPSs were accomplished by a bidirectional voltage sweep from 0 mV $\rightarrow$ -1 mV $\rightarrow$ 0 mV $\rightarrow$ 1 mV $\rightarrow$ 0 mV. To avoid unwanted short circuits overloading the system with current, a compliance limit was set, which is the maximum allowed current to pass through the system, equal to 1 mA.

In the earlier work with two-wire measurements, one of the major challenges was to keep the measurement system stable, due to bad adhesion between the particles and the silver paint used. Both the AgPS and the probes moved between the repeated measurements done on the same system. This resulted either in a increasing resistance or the complete loss of electrical contact. As a consequence, especially in the latter case, the probes had to be re-indented. This caused very variable measurements for the thinnest film 60Ag.

With the renewed preparation method, Section 3.2.1, the AgPSs were better attached to the substrate. This combined with a gentler probe approach and more efficient measurements should give more consistent results.

3.4.3 *Four-wire Measurements*

The same equipment was used for the four-wire measurements as for the two wire setup with the exception of adding a second pair of probes. The second pair was, as explained in Section 2.5.2, there for voltage drop measurements while the other pair supply current. The full setup can be seen in Figure 3.5.

The placement of the probes was more critical when an additional set of probes was placed on the sphere. The best four-wire measurements were achieved when the voltage measurement probes, V-probes, were as close to the current probes, I-probes, as possible, but without touching. Due to the miBot setup, the V-probes had to be introduced from the sides, Figure 3.4. A close up of one sphere measured with this approach, can be seen in Figure 3.6. For four-wire measurements to give reliable results, it was also important that the probes were placed without interfering with the already placed probes, causing them to loose contact.

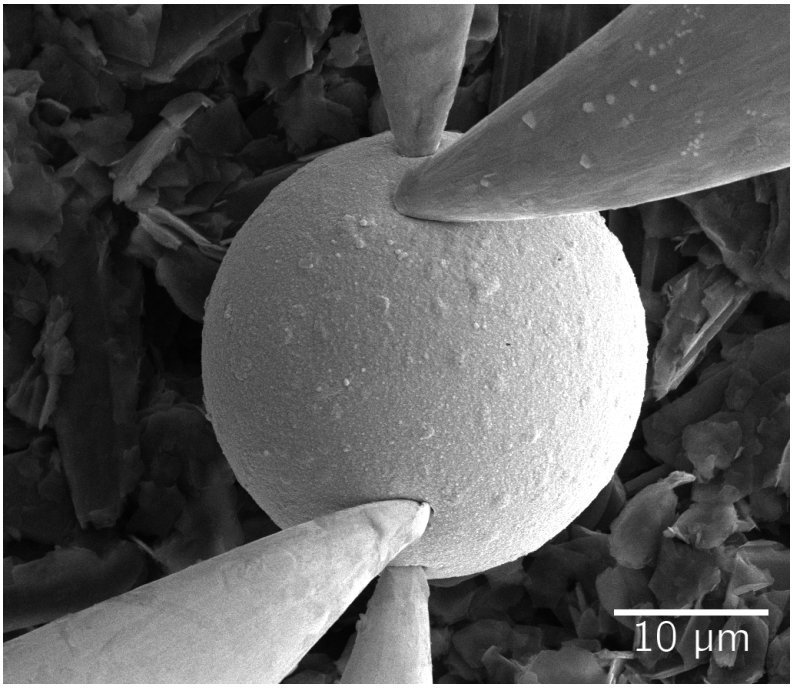

Figure 3.6: A four wire measurement of a 150Ag. The probes from north to south are the current transporting probes, while the probes from the sides measures the potential.

A bidirectional voltage sweep was applied over the two I-probes in Figure 3.5 to induce a current over the sphere. The sweep went from 0 µV → -200 µV → 0 µV → 200 µV → 0 µV. The compliance limit was set to 5 mA. The resulting I-V curve was saved and later processed.

3.4.4 *Data Processing*

The I-V curves stored from the two- and four-wire measurements were processed with the help of a Matlab script, Appendix B. The script makes a linear fit to the the I-V sweep and finds the resistance from the slope as explained in Section 2.5.2. The measurements which were clearly out of bounds by a magnitude or more were removed from the final evaluation. The reason for omitting some of the measurements were either because the visual state of the particle or particle-probe interface was not consistent, i.e. creep, damage or contamination, or because the resulting I-V curve indicated poor electrical contact.

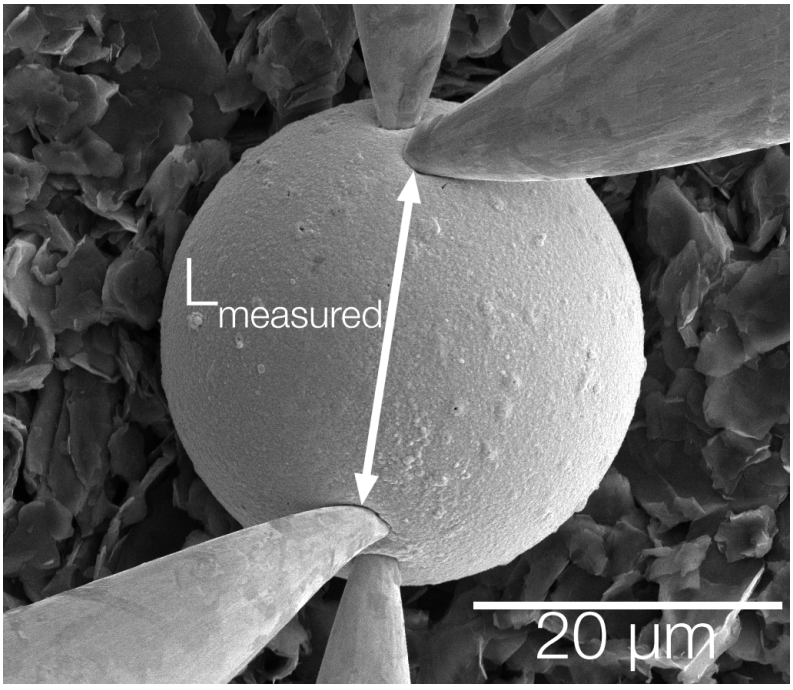

Figure 3.7: Measuring of the V-probe distance. The shortest distance between the probes are measured, white arrow.

The distance between the probes were found by relating the scale bar to the pixels in the SEM picture of the setup in the image analysis software *ImageJ*[2]. The distance was measured from the tip from one of the V-probe's contact with the coating to the next, see Figure 3.7. This distance, $L_{measured}$, was related to the arc length, L_{arc}, of the

2 Documentation can be found at `http://imagej.nih.gov/ij/index.html`.

silver coating by the simple relation in Equation 3.1. D and t being the polymer sphere diameter and coating thickness respectively.

$$L_{arc} = (D + t) \arcsin\left(\frac{L_{measured}}{D + t}\right) \tag{3.1}$$

3.5 RESISTANCE SIMULATION

The resistance over the AgPS surface was simulated in *COMSOL Multiphysics 5.0*. The software was used to create a geometrical 3D model of the sphere and perform electrical simulations. The software allows for multiple physics to interact and be simulated at the same time through a series of converging differential equations. For the current simulations, only the AC/DC module was employed.

The model consists of multiple modules to build a complete model: The geometry module defines the geometrical boundaries and appearance of the model. The material module defines which materials the different parts of the model consists of and their respective properties. The electrical module defines the electrical properties and influences. The mesh module defines the resolution of the differential equations to be solved. And the solver module defines the type of solution to be calculated e.g. stationary solution.

3.5.1 *The 3D Model*

The 3D model was created to imitate the AgPS in an efficient way. The finished drawn model for the 270Ag can be seen in Figure 3.8. The core was of PMMA, exposed as yellow in the figure, and have a diameter of 30 μm. The gray silver film covering the PMMA was adjusted to the different film thicknesses. In the case of Figure 3.8, the thickness is set to 270 nm. The current probes (I-probes) of tungsten (W) were placed on opposite sides of the upper sphere cap. They were indented ~ 80 % into the film. This was not done as a simulation, and they were fully indented in the initial geometry. Thus the model consists of three domains; a sphere and two probes. The latter coupled to the sphere by the definition of a electrical contact, see Section 3.5.2.

The sensing probes (V-probes) were represented as the intersection between the sphere cap at about 10 μm on the z-axis and the line along the x-axis that also intersects with the I-probes, red dots in Figure 3.8. As the current through the V-probes was negligible compared to the current between the I-probes, the contact area between the V-probe and the silver coating was not important, and they are therefore

represented as measuring points rather than real probes for simplicity. The distance between the V-probes was taken as a average of the V-probe distance from the real four-wire measurements.

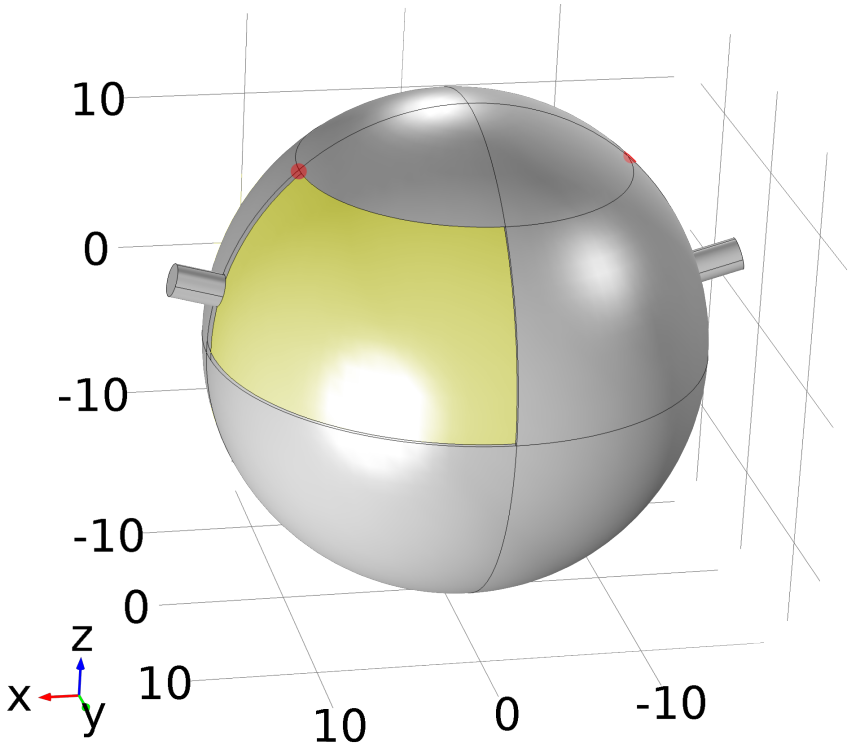

Figure 3.8: The 3D model drawn with the *Geometry* module in COMSOL. The scale on the axes are in μm. A piece of the silver film is removed to expose the PMMA core (yellow). The red dots marks the placement of the V-probes.

The mesh of the model was first defined by the built-in physics controlled mesh generator in COMSOL. The model was first run with a normal sized mesh, and then at a fine mesh and ultimately a finer mesh to see if the results converged towards one answer. The mesh was then tailored to make the model efficient for simulations. The most critical points, such as where the I-probe indents the coating, were given a very fine mesh. The larger parts of the coating were given a rougher resolution, with the goal to achieve both an efficient and precise model.

3.5.2 *Electrical Domains*

Still referring to Figure 3.8, the current was set to travel through the system by setting up a potential of 200 μV between the outward facing circular ends of the cylinders representing the current transmitting probes. These probes wetr paired in an electrical contact with the

silver film. In the contact area, the silver film was given the material properties of surface roughness and slope based on AFM investigations as well as a microhardness value from literature at 1.2 GPa [30]. Both the end and the sides of the probe in contact with the film, was able to transport current and were included in the contact area. The polymer core was set to not be a part of the electric node, thus the current will only move through the probes of tungsten and the silver film.

When placing the probes on the AgPS with the miBots, the miBots do not offer any force or displacement control. The miBots have a maximum holding force of 0.2 N, which applied on a flat punch probe 2 μm in diameter, equals a pressure of 64 GPa. It is difficult to know the amount of force applied from the probes to the silver film that results in approximately 80 % indentation, since the coating fails long before this pressure. This force have an impact on the contact between probe and film and was therefore obtained from another simulation[3].

3.5.3 *Resistance Evaluation*

To evaluate the resistance, a current was induced by an external potential over the I-probes. The potential over the sphere was measured at the two points marked with red in Figure 3.8, representing the V-probes. To set the distance between the V-probes in the model, the average distance from the corresponding experimental measurements was calculated. Ohm's law was applied to find the apparent resistance on the coating between the voltage probes by dividing the voltage drop by the terminal current obtained from the simulation.

3.5.4 *Resistivity*

The electrical properties of the silver coating in the simulations are based on the standard bulk resistivity of silver, $\rho^{bulk} = 1.51 \times 10^{-8}$, given by COMSOL. The resulting resistance from these simulations, R^C, relates to this resistivity as the measured resistivity, R^E, relates to the apparent resistivity of the real AgPS, $\rho^{E\star}$. The relation between R^E and R^C gives the thickness dependent relation $\alpha(t)$, as seen in Equation 3.2.

$$\alpha(t) = \frac{R^E}{R^C} = \frac{\rho^{E\star}}{\rho^{bulk}} \tag{3.2}$$

3 This mechanical simulation is done by Sigurd Pettersen and is part of his Ph.D. thesis [31]. The pressures used is presented in Table 5.1

With this approach, the apparent resistivity $\rho^{E\star}$, of each coating thickness is calculated with Equation 3.3.

$$\rho^{E\star} = \rho^{bulk}\alpha(t) \tag{3.3}$$

3.6 AFM

The surface topology of the AgPSs were studied with the help of an *AFM Veeco multimode V* from BRUKER. The AFM was operated in the QNM mode with automated settings in the accompanying software *NanoScope 8.15* also from BRUKER. The MPP-13120-10 probe with spring constant 200 N/m, resonant frequency 525 kHz, a rotated tip with 8 nm radius, and aluminum reflective coating was used combined with the type E piezo scanner.

3.6.1 *AgPS Sample Setup*

The samples were prepared as described in Section 3.2.1 and 3.2.2. The AgPSs have a diameter of 30 µm which was out of bounds for the vertical displacement of the AFM probe. Therefore, in order to scan the sphere surface, the AFM tip had to be manually placed directly over one sphere by changing the position of the AFM head over the stationary sample and scanner before scanning. This was achieved by the help of a video camera mounted above the AFM tip and sample. The tip was lowered further manually to some hundred of microns above the surface, before the software-controlled piezo scanner lifted the sample the remaining distance. If the AFM tip successfully made contact with a AgPS, a image was produced with the settings in displayed in Table 3.1. For each sphere, one picture was produced. Only the 100Ag spheres were investigated, as data from the other coating thicknesses already were obtained with the exact same method and parameters [31].

3.6.2 *AFM Analysis*

The AFM height data were processed with the *NanoScope Analysis v1.50* software from BRUKER. With the help of internal functions in the software, the RMS surface roughness and RMS surface slope were calculated. The RMS values were calculated both before and after the height data image was flattened. The surface flattening was done with a 3rd order function which fits each line individually to the center data, and removes the tilt and bow. The result was flattening of the

Table 3.1: The image settings for the AFM Veeco during scanning of the AgPS surface.

Image Settings	
Scan size	1 μm × 1 μm
Samples/line (pixels)	768
Size/pixel	1.3 nm
Scan rate	0.651 Hz
Peak force amplitude	auto
Gain	auto

sphere curvature, but may also include some of the actual topological features. Both the raw and flattened data is therefore included in the results.

4 RESULTS

In this chapter the results from the surface investigations of the four different AgPSs are presented, both visual inspection with SEM and investigations done with AFM. This is followed by a brief comment about the sample preparation and probes, before the measurement sections: The first describes the results from the simplest two-wire method with micromanipulators setup, Section 4.3. This is followed up by the more accurate four-wire method, Section 4.4, where also some of the computer modeled results from COMSOL are included. The major part of the COMSOL simulations is presented in Chapter 5.

4.1 SILVER-COATED POLYMER SPHERES

Since all the AgPSs consist of the same materials and were prepared in the same way, their physical properties should only be related to the process of making the silver coating thicker or thinner. SEM pictures as well as AFM recordings are provided to account for how the surface topology changes with the coating thickness.

4.1.1 *Surface Features*

the measurements performed on the AgPSs were supervised through a SEM. The SEM is a powerful characterization instrument that can be used to investigate the particles at high magnification, not just to ensure the probes are in the right place. The detection of backscattered secondary electrons, see Section 2.2.2, makes it possible to see both topography, atomic contrast (Z-contrast) and channeling contrast. Since the material should be mostly silver, topography and channeling effects are most interesting.

Figure 4.1 presents SEM pictures taken at high magnification of all the different coating thicknesses. It is evident that different silver thicknesses results in different topography and morphology. The 60Ag in Figure 4.1(a) has small distinct grains ~100 nm in diameter probably in a monolayer, as the dark PMMA in between the grain

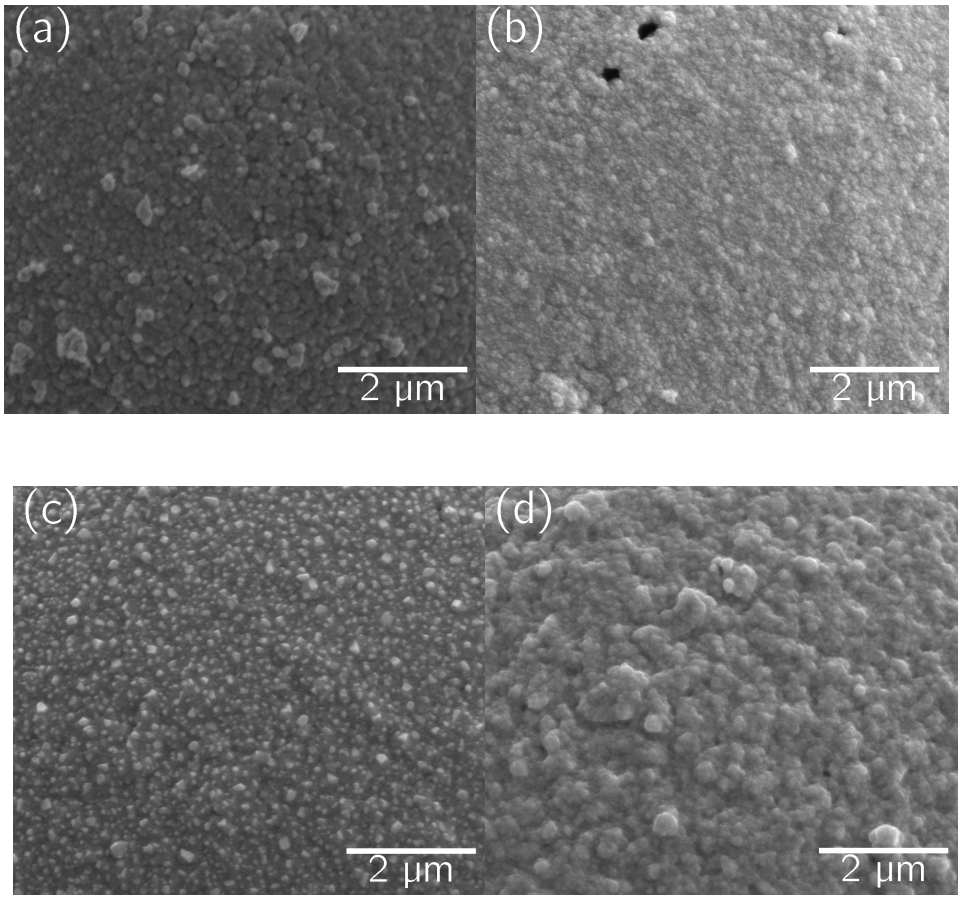

Figure 4.1: Close up SEM pictures of the surfaces of all the different AgPSs investigated in this project. (a) shows the 60 nm Ag coating, termed 60Ag and (b), (c), and (d) show the 100Ag, 150Ag, and 270Ag coatings respectively.

boundaries is just visible. The coating seem however to be continuous in the large majority of the spheres, but often with some distinct larger features in the form of debris on top of the coating. The 100Ag has a what seems like a more uniform and uninterrupted coating. The dark lines between the grains are no longer visible. The holes seen in the top left of Figure 4.1(b) can be seen in both 60Ag and 100Ag, but they seldom appear larger than 100-300 nm in diameter. These holes have not been observed in thicker coatings.

Figure 4.1(c) shows the 150Ag as having a smooth surface much similar to the 100Ag, but the morphology is somewhat different. Small dots on the silver coating emits significantly more SE/BSE than the surroundings. This indicates a different morphology in these areas. The same bright grains were also sometimes observed in the 60Ag and 100Ag as well. The 270Ag in Figure 4.1(d) really stand out when

it comes to topology. It has multiple layered grains of different sizes causing a rough uneven surface.

4.1.2 *Mechanical Observations*

The miBots's probe indenting of the different AgPS has led to some general qualitative observations of the mechanical properties. The thinner films, as the 60Ag and 100Ag and to some extent 150Ag show a mechanical behavior as expected from a polymer, see Figure 4.2(a). This made the spheres easier to clamp between to probes without them escaping when placing the 3rd and 4th probe. The thick silver coating in 270Ag and to some extent 150Ag, caused the spheres to behave more like a ductile metal, Figure 4.2(b). That made it harder to keep the probes in place on the sphere when the second pair of probes was introduced. A combination of an increased force upon indentation to make contact with the rough thick coating and the metal properties of the coating, lead to a sliding motion, thus loosing contact with the already placed probes. This was especially a problem when the AgPS was poorly attached to the substrate.

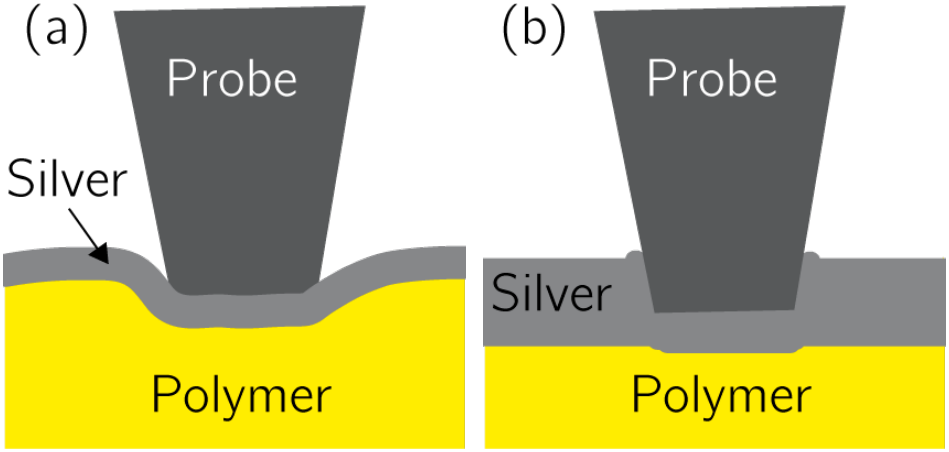

Figure 4.2: The different coating thicknesses seem to behave different upon indentation of the probes. The thinner coatings like 60Ag and 100Ag show a behavior much like the PMMA core, (a). The thicker 270Ag in (b) seem to behave more like a ductile metal.

4.1.3 *AFM Results*

The topographical observations of the AgPSs using the SEM could be confirmed by the AFM measurements. All the measurements were

performed with the same setup, described in Section 3.6.1. The raw data from the AFM often look like in Figure 4.3(a), with a slight curvature and tilt. This is normal considering the surface being part of a sphere, as well as the the tilt being a common error in AFM. After being flattened, the topology become more prominent, as seen in Figure 4.3(b). Both the raw data and the flattened results are used further in the evaluation of the surface topology.

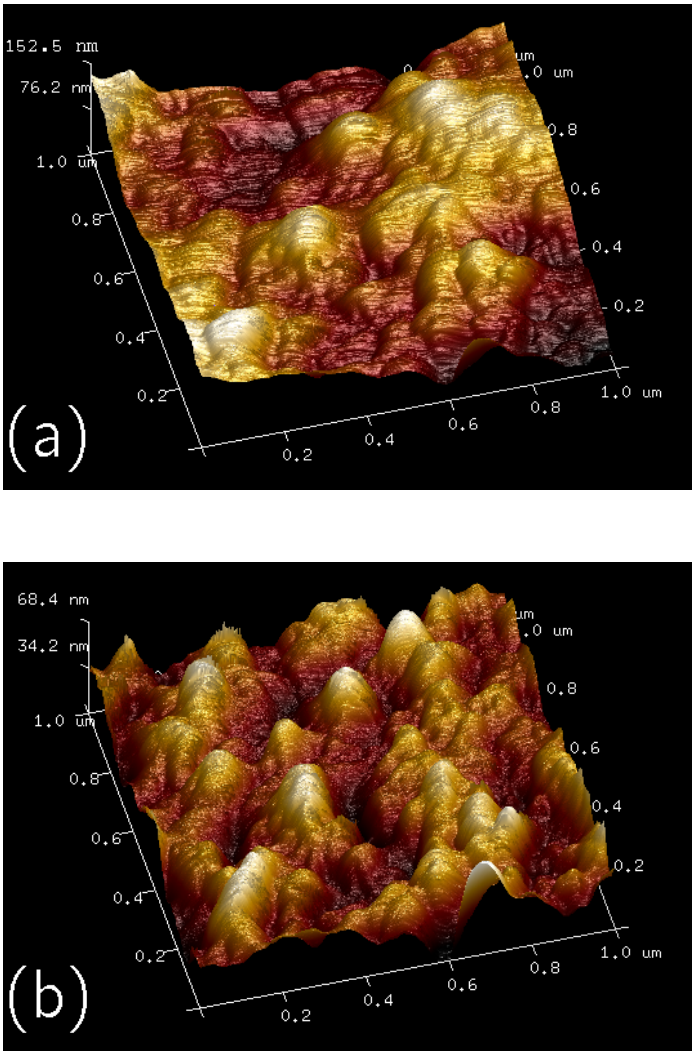

Figure 4.3: A three dimensional representation of the AFM results talen from a 1 µm × 1 µm area of a 100Ag. The graph in (a) shows the untreated data. In (b), the a 3rd degree flattening function is applied to eliminate the image plane curvature.

The results form the RMS surface roughness, Figure 4.4[1], was as expected when it came to increasing values with increasing coating thickness. That the deviation also increases, fits with the chemical deposition method, as more random deposition leads to a wider distribution of topologies. The flattened surface roughness data gave a more conservative development as curvature and tilt were removed.

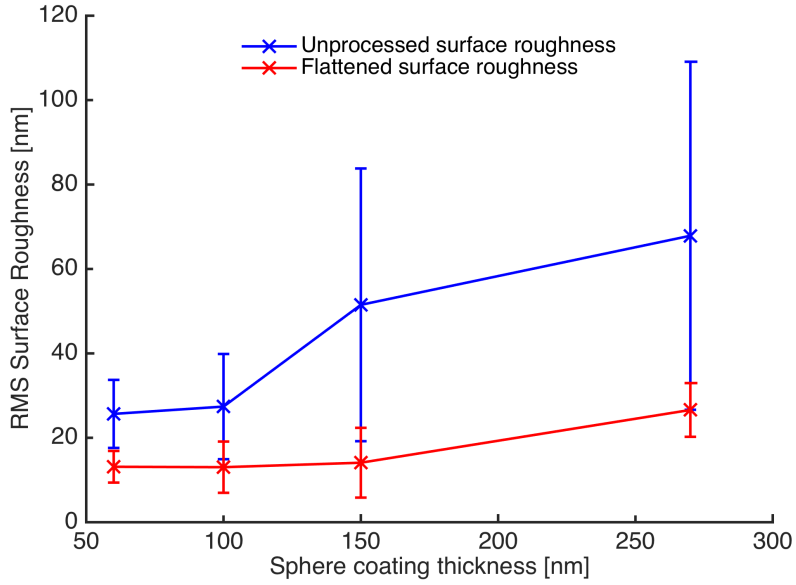

Figure 4.4: The RMS surface roughness is increasing with thickness. For the unprocessed AFM data, there is a big increase from 100Ag to 150Ag. When the AFM data is flattened as in Figure 4.3(b), the three thinnest coatings have quite similar roughness, the transition being between 150Ag and 270Ag.

The RMS surface slope for the different coatings in Figure 4.5[2] show a different trend than the RMS surface roughness. The thinnest and thickest coating have twice as steep slopes than the two intermediate thickness coatings. The steep slope recorded for the 60Ag was a result of non existent high peaks recorded. These peaks are artifacts caused by the AFM tip not being able to follow the sample. The artifacts were not corrected for in the results presented here. The exact figures for roughness and slope are displayed in Table 4.1.

1 The AFM results for the 60Ag, 150Ag, and 270Ag are recorded by Sigurd R. Pettersen and will be part of his Ph.D. thesis. [31]

2 The 60Ag, 150Ag, and 270Ag results are also a part of Sigurd R. Pettersen's Ph.D. thesis. [31]

Table 4.1: A summary of the RMS values. The each value represent an average of 4-6 separate AFM measurements.

	RMS surface roughness		RMS surface slope	
Thickness	Unprocessed	Flattened	Unprocessed	Flattened
60 nm	25.7 nm	13.1 nm	1.67	1.51
100 nm	27.4 nm	13.0 nm	0.65	0.57
150 nm	51.5 nm	14.1 nm	0.78	0.58
270 nm	67.9 nm	26.6 nm	1.77	1.54

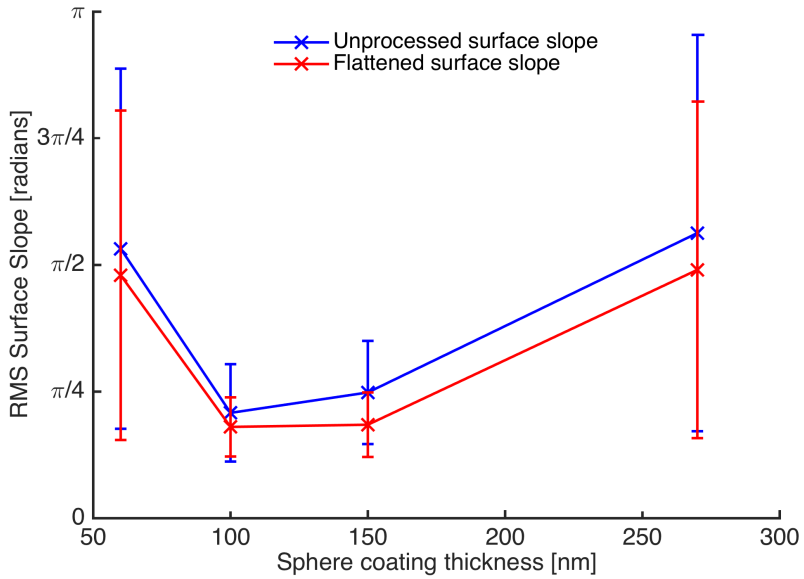

Figure 4.5: The RMS surface slope have fairly similar development for both the unprocessed and flattened AFM data, the latter have as expected a bit lower values due to the flattening. The slope is most prominent in the extremes; 60Ag and 270Ag.

4.2 Sample preparation and probing

The LEIT-C Carbon Cement (CC) was used to fasten all types of AgPSs to the Si substrate. The preparation method gave samples of good quality, but the distribution of CC was sometimes too uneven, making it hard to access the spheres with the probes. Poorly sprinkled spheres could also make them unaccessible for measuring because of agglomeration.

Figure 4.6 is a typical view of how one part of a prepared sample look like. There are some areas with agglomeration or cluttered spheres (middle left), which would be hard to access with the probes.

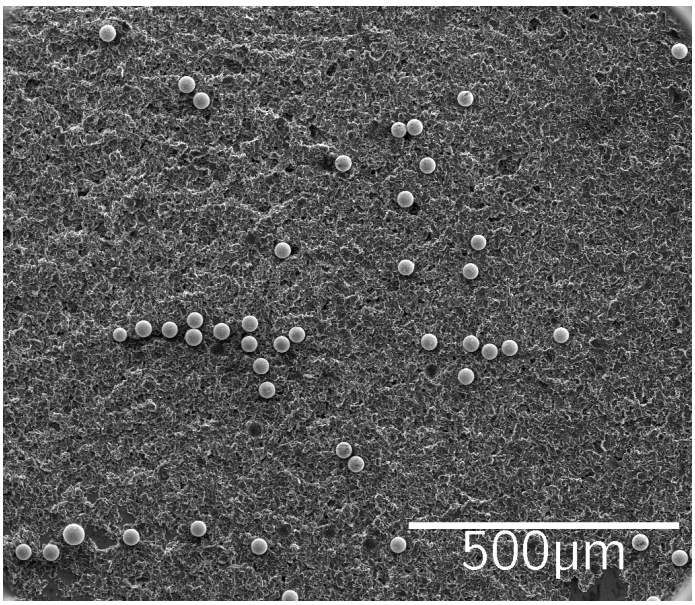

Figure 4.6: 60Ag spheres on a prepared sample sample of Si with Carbon Cement (CC).

The single spheres were most accessible if they do not have any carbon cement structures nearby, obstructing the probe's path. An ideal placement of an AgPS can be seen in Figure 4.7(a), where both placement and surface adhesion match.

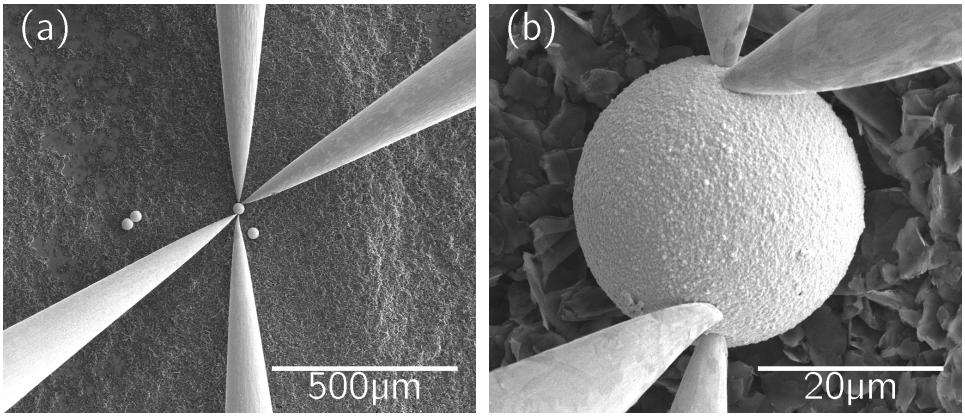

Figure 4.7: (a) is an overview of how the probes are placed in a four-wire setup. (b) shows a close up of the contact with the AgPS is done.

4.2.1 *Probes*

When placing the probes, the contact area must be taken into consideration to achieve good results. The probes transporting current,

I-probes, should have good electrical contact, but they should also have a good contact area to minimize contact resistance (voltage drop), Figure 4.8(a). This is especially important in two-wire measurements where the contact resistance is included in the measured total resistance. In the case of four-wire measurements where the voltage measuring probes, V-probes, are separate, only electrical contact is important, as no current is to be transported. For the majority of the four-wire measurements, probes with a contact area of ~2 μm was used for both probes Figure 4.7(b). But for characterization of particles smaller than 30 μm, smaller V-probes have proved successful. The setup for 10 μm AgPS utilize two V-probes that have a slimmer profile and smaller contact area, Figure 4.8(b).

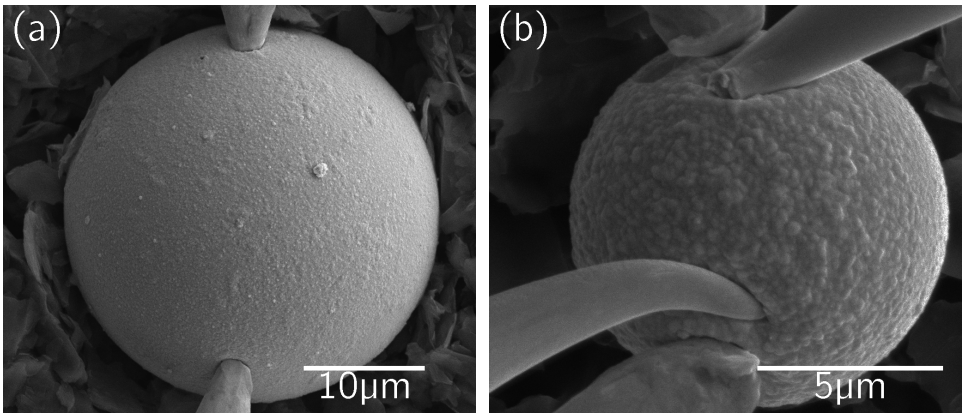

Figure 4.8: The normal probes with ~2 μm diameter flat punch area in a two-wire setup in (a). The special four-wire for small spheres, (b). A thinner version of the tungsten (W) probes are used to measure the voltage. The normal sized probes are used for current.

4.3 RESISTANCE MEASUREMENTS BY THE TWO-WIRE METHOD

The simplest way of doing resistance measurements, is by the two-wire method. This have proven useful for a proof of concept (the miBot setup) and for troubleshooting more complicated measurements. Earlier two-wire measurements performed with the miBot setup presented in Section 3.4.2, were not very consistent and no proper investigations were done in order to remove the internal system resistance from the results. The two-wire measurements were therefore repeated and are presented below.

4.3.1 *Measuring internal Resistances*

The internal resistance of the system was measured by removing the W-probe from one miBot and then connecting this miBot with another miBot using one common W-probe. Hence, the W-probe was used as a conducting bridge between the two miBots, creating a closed circuit for a two-wire measurement. A normal voltage sweep was done on this system. The result was a very consistent output of 6.41 Ω. This internal resistance is subtracted from the two-wire measurements after calculating the total resistance in the next section.

From the manufacturer of the miBots, IMINA TECHNOLOGIES, each miBot with a W probe was assigned a resistance of $R_{probe} = 3.5\ \Omega$ and the circuit should have an resistance of $R_{circuit} = 5.2\ \Omega$, giving a total internal resistance of $R_{Int,Imina} = 12.2\ \Omega$. This is twice as much as measured, $R_{Int,measured} = 6.41\ \Omega$.

4.3.2 *Measured Resistances*

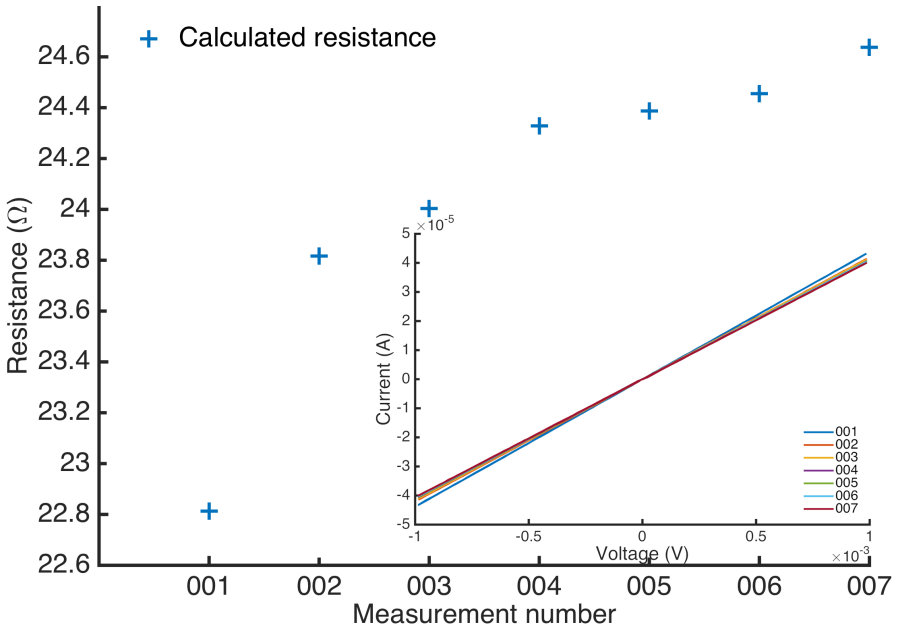

Figure 4.9: Seven consecutive measurements done on the same 100Ag sphere. Each "+" corresponds to an I-V curve slope from one measurement seen in the insert. The measurements are taken at a 15 second interval.

The seven consecutive measurements done with the two-wire measurement method on the same AgPS, have shown the resistance to increase with the number of measurements. Since the increase in resistance is though to be a consequence of the measurement, the first

measurement was used to represent that particle in further analysis, Figure 4.9. The remaining six are therefore used as reference for the measurement quality: A large deviation from the first measurement, indicates a problem with either the probe placement or film quality. The results from these observations, are that all the measurements had an increasing resistance with the number of measurements. It is important to note that the probes were not moved after they were indented and the measurements begin. This was especially challenging with the 60Ag, which is softer than the other spheres, Section 4.1.2.

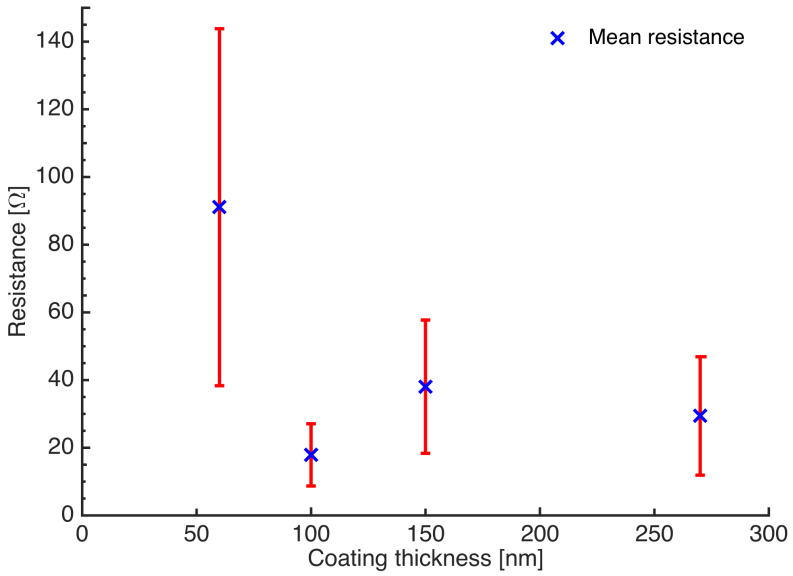

Figure 4.10: The mean resistance of AgPSs calculated from the first obtained I-V curve from each sphere. The I-V curves were obtained by 2-wire measurements. The red error bar shows the standard deviation in the resistance mean, marked with a blue "x". The resistance is based upon eight individual sphere measurements for each thickness.

The result of all the first measurements gathered can be seen in Figure 4.10. A couple of rare case measurements where the measured resistance were over 300 Ω was removed from this last evaluation, since they were found to be caused by impurities on the probes. The 100Ag received the overall lowest resistance, Table 4.2. This is surprising, since the other spheres are part of a more logical development where the resistance decrease steady with increasing coating thickness. This means that the resistance measured is not related directly to the film thickness for the two-wire measurements.

Table 4.2: The mean resistance with accompanying standard deviation of the AgPS measured with the two-wire method. The numbers corresponds to the results presented in Figure 4.10.

Coating Thickness	60Ag	100Ag	150Ag	270Ag
Mean Resistance [Ω]	91.1	17.9	38.0	29.4
Standard Deviation [Ω]	52.7	9.2	19.7	17.5

4.4 RESISTANCE MEASUREMENTS BY THE FOUR-WIRE METHOD

A four-wire setup is thought to be the best method for finding the resistance of the AgPS, thus fulfilling the main scope of this project. The method is described in Section 3.4.3 and Section 4.2, so this section will present the results from the four-wire measurements. Simulations in COMSOL were performed for comparison to the measured results and are included here. Further elaboration of the COMSOL results will be presented in Chapter 5.

4.4.1 *Measured Resistance*

The resistance measurements proceeded in basically the same manner as for the two-wire measurements: I-V curves were produced and analyzed. However, with two more wires complicates the measurement procedure and troubleshooting for errors in the measurements were more difficult. Lack of output can easily be solved by two-wire measurements of the separate probe pairs, see Appendix A. Though, it was often difficult to know the cause of other faults or irregularities when using the four-wire procedure.

The output of the curves from the four-wire measurements seem more tangled and noisy. To achieve perfectly straight I-V curves was not possible. Almost all obtained measurements show signs of hysteresis either at negative voltage, positive voltage, or both. However, the results have been interpretable by the same curve fitting method as for the two-wire measurements. An example of one of a high quality collection of I-V curves can be seen in Figure 4.11(a). There is always a little drop in the current feedback either on the way up or down from the voltage extrema. This is visible in Figure 4.11(a) on the way upwards from -200 μV.

The I-V curves in Figure 4.11(b) look fuzzy and the current drop seen in -100 to -50 μV area is much more substantial. The rest of the curve has an even slope. All the consecutive measurements had the same development, so this current drop creating the hysteresis must

have something to do with either the probe placement and contact or the properties of that specific coating. The linear fit performed on these curves will result in a slightly lower slope because of the current drop. This results in a higher calculated resistance.

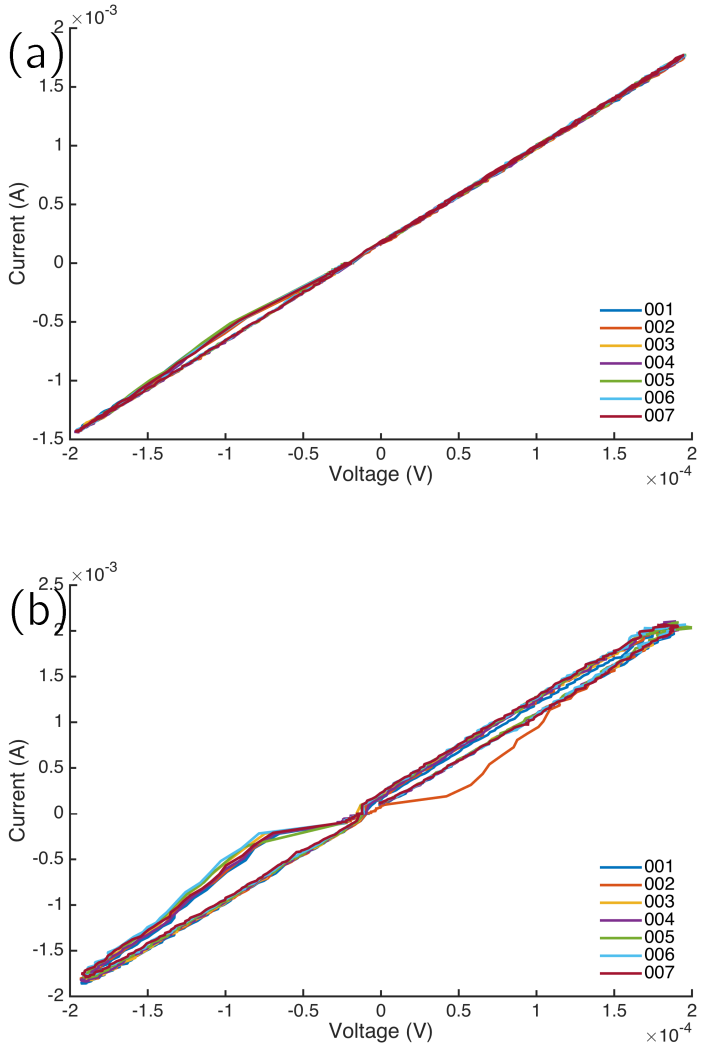

Figure 4.11: I-V curves taken from four-wire measurements of 100Ag. One system equals one AgPS. The curves in (a) have a very straight appearance except for one little hysteresis on the way up from -200 µV. The curves in (b), have a larger hysteresis. The curve representing measurement 002 (orange) show both a hysteresis on the way up and down.

The resistance derived from the two sets of I-V curves in Figure 4.11 are displayed in Figure 4.12. When compared with the two-wire measurements, neither of the four-wire measurements had a similar monotonic and unambiguous increase of the resistance with time. This is true for all the measurements, and is exemplified in Figure 4.12. The

blue "+" which denotes the calculated resistance from Figure 4.11(a), have a monotonic decreasing development. The red "x" corresponding to Figure 4.11(b), developed into a parabola. Interestingly, the most perfect I-V curves results in the highest resistance. The fuzzy curves averaging at ~0.15 Ω below. The blue data set had the advantage of being taken with a V-probe distance of 17 μm, contrary to the V-probe distance of 25 μm for the red "x's". This means that the negative effect of having a bit fuzzy and not ideal I-V curve is not larger than normal deviation in resistance between two AgPS with the same coating thickness.

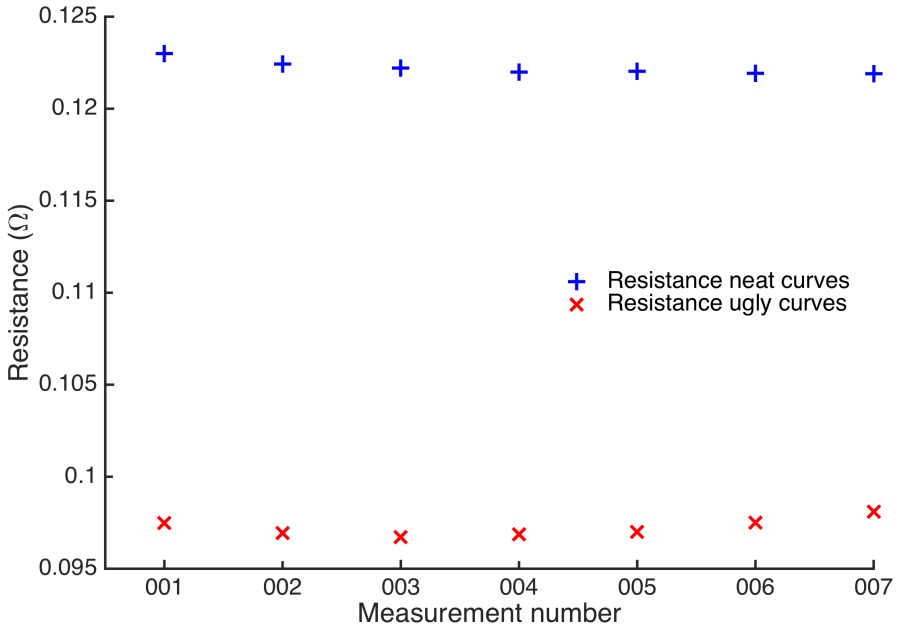

Figure 4.12: The blue "+" represent the resistances corresponding to the I-V curves in Figure 4.11(a), having an mean resistance of 0.12 Ω. The red "x" marks the resistance of the I-V curves in Figure 4.11(b), with an mean of 0.97 Ω.

The mean resistance from each measured sphere is represented as a mean in Figure 4.13, the exact values are presented in Table 4.3. The statistical right way to represent the deviation between the measurements performed on the same AgPS, is the standard error of the mean (StEM). The StEM is the standard deviation of the mean of the means. This is a result of the *Central Limit Theorem*, and the StEM is found by taking the sum of the standard deviations of the means divided by the square root of the number of means [32, chap. 8.4]. But as the StEM turned out to be too small (0.0002-0.002 Ω) to be visible in Figure 4.13, a simple standard deviation between the means were calculated for each type of AgPS, not taking the standard deviation from each sphere into account.

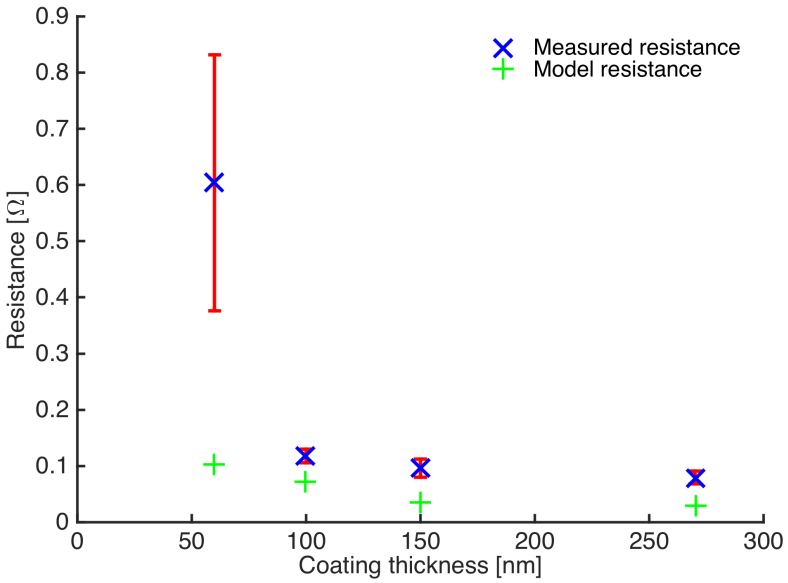

Figure 4.13: The blue "x" represent the mean of all the means taken from the corresponding AgPSs. The red error bar represents the standard of the means. All measurements are done with the four-wire method. The green "+" markers denote the modeled resistance obtained from using the same geometrical parameters as for the real measurements and table values for physical constants. 270Ag is based on seven individual sphere measurements, the others on eight.

Table 4.3: The mean resistance with accompanying standard deviation of the AgPS measured with the four-wire method. The numbers corresponds to the results presented in Figure 4.13. The mean V-probe distance for the different AgPS are also included with accompanying standard deviations.

Coating Thickness	60Ag	100Ag	150Ag	270Ag
Mean Resistance [Ω]	0.604	0.118	0.096	0.079
Std. Dev. Resistance [Ω]	0.228	0.012	0.016	0.011
Modeled Resistance [Ω]	0.104	0.072	0.035	0.028
Mean V-probe Distance [μm]	23.35	25.70	20.40	26.74
Std. Dev. Distance [μm]	2.99	2.74	2.35	2.44

The standard deviation is overall small compared to the two-wire results where the deviation constituted over 50% of the mean resistance. For the four-wire measurements, this is around 15% with the exception of 60Ag which is almost 40%. The four-wire measurements

were thus more consistent and less variable. As demonstrated in Figure 4.8(b), a four-wire setup with smaller V-probes on a 150Ag with a diameter of 10 µm was tried out. Two different spheres were measured as a proof of concept, averaging at 0.082 Ω. This places the spheres in between the 30 µm 150Ag and 270Ag in Table 4.3.

4.4.2 *V-Probe Distance*

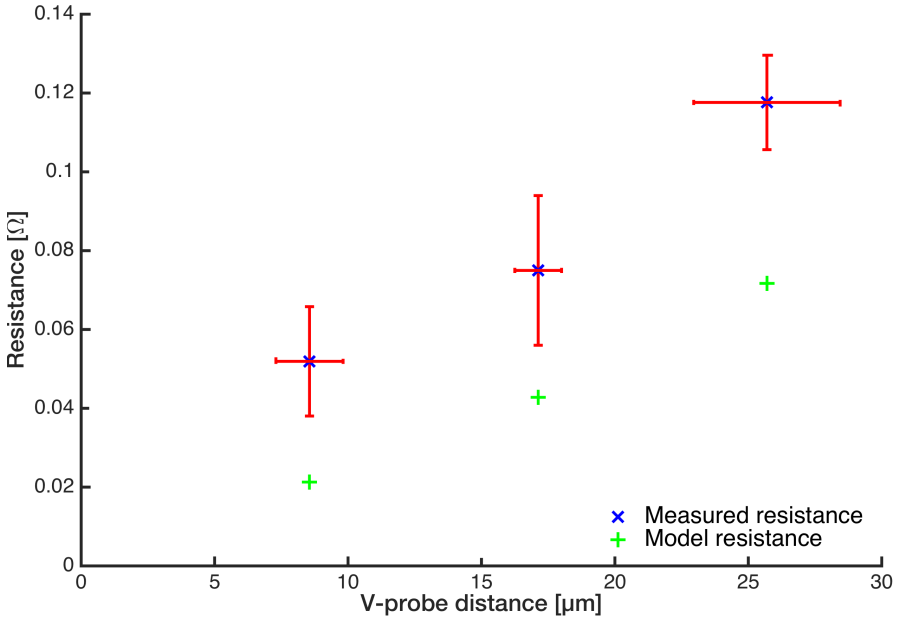

Figure 4.14: Resistance investigated on the 100Ag with four-wire measurements by varying the distance between the two V-probes, the mean is marked with a blue "x". The horizontal error bars represent the standard deviation in the distance between the V-probes, the vertical represent the standard deviation in resistance. The green "+" marks the resistance obtained from the COMSOL model using the same geometrical parameters as for the real measurements and table values for physical constants. The longest V-probe distance measurements are based on data from eight spheres, the two shorter on five each.

The resistance is a property dependent on the geometry of the sample. It would therefore be interesting to find out how the distance between the voltage measuring probes would affect the resistance output. The results of these investigations are presented in Figure 4.14. The blue "x" marks the average resistance at the average corresponding V-probe distance. The standard deviation of the distance is given as the horizontal error bar, the vertical error bar denotes the standard deviation of the measured resistance. While the resistance overlap

somewhat between the two shortest distances, the V-probe distance has a minimum of 4 μm distance between any two independent observations.

The COMSOL model results of the same measurements had a trend quite similar to the four-wire measured results. Since the only change between each measurement, in the model as well as with the miBot probes, was the V-probe distance, it can be assumed that the difference was caused by different material constants, in this case, the silver conductivity. An estimate of the conductivity for the different AgPSs could then be found by Equation 3.2 and 3.3. See Section 4.4.3 for the detailed results of this evaluation.

The mean resistance for the largest V-probe distance in Figure 4.14 have a smaller deviation in the resistance compared to the smaller V-probe distances, despite having the largest deviation in distance. This indicates that it was an advantage to have the I-probes as close to the equator as possible and the V-probes being as close to them as possible to get the most stable results.

4.4.3 *Resistivity*

The resistivity of a material can be used to compare the material's electrical properties relative to each other materials, independent of geometry. The similar trends seen both in the measured and modeled resistance, makes it possible to relate the resistances in order to find the apparent resistivity, Equation 3.2. The results from these calculations are listed in Table 4.4. This approach resulted in the second thinnest coating 100Ag, to have the lowest resistivity. The a priori assumption was that the resistivity should be constant, however, the results in Figure 4.15 indicate that this was not the case. Both 60Ag and 100Ag deviates significantly from 150Ag and 270Ag. As seen in Table 4.3, there were some variation in the mean V-probe distances for the different coating thicknesses, but the standard deviation was about the same. There was no clear correlation between the 100Ag resistance and the V-probe distance that could cause the lower resistivity. If that was the case, should this effect be seen in resistivity for 270Ag as well.

Table 4.4: α is found by Equation 3.2 and gives the relation between the bulk conductivity and the apparent resistivity of the AgPS, Equation 3.3. The apparent resistivity is also plotted in Figure 4.15.

Coating Thickness	60Ag	100Ag	150Ag	270Ag	Bulk
α	5.82	1.63	2.74	2.81	1
App.Resistivity[Ωm]	8.81e-8	2.47e-8	4.14e-8	4.42e-8	1.51e-8

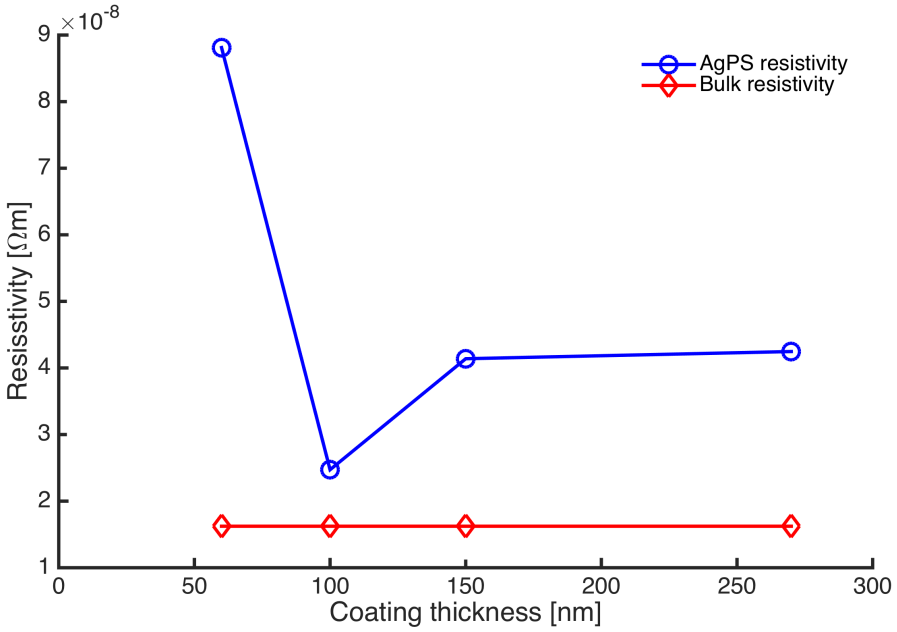

Figure 4.15: The bulk resistivity of silver, marked with a red "◇", is used in the COMSOL model for calculating the resistance. Relating the measured resistance to the modeled resistance like in Equation 3.2 and 3.3, the resistivity for each AgPS was obtained marked with a blue "○".

5 COMSOL SIMULATIONS

COMSOL Multiphysics models are based on solving multiple differential equations for small domains of the model. All these small pieces are combined into covering the whole geometry to be modeled, called a mesh. The size of the domains in the mesh can be changed, smaller domains may give a higher precision, but demands much more computing power. To confirm the model results presented in Figure 4.13 and 4.14, the mesh size was decreased until the three first digits converged. An excerpt of the mesh used in the final model can be seen in Figure 5.1. This mesh have approximately 230 000 elements with a minimum element quality 0.03546.

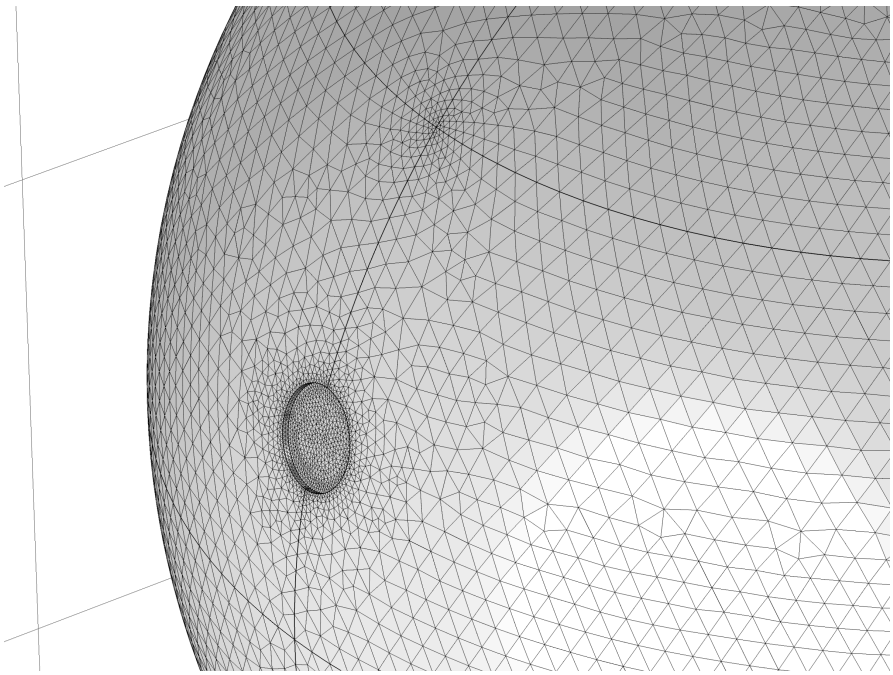

Figure 5.1: The mesh used in the COMSOL Multiphysics simulations. The high impact regions in the silver coating around the I-probes (removed from this picture) and in the area where the voltage is recorded, have a finer mesh.

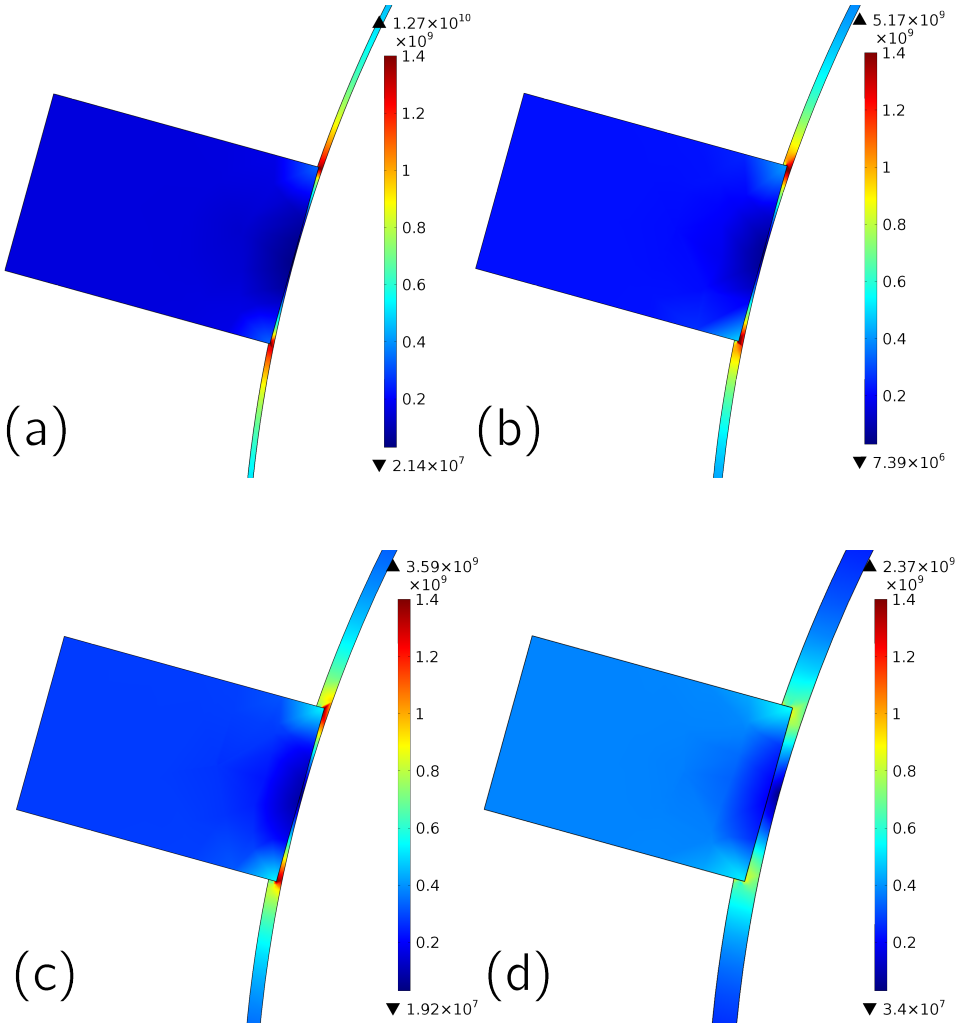

Figure 5.2: The modeled current distribution in the silver coating around the terminal probe for all four coating thicknesses. (a) is the 60Ag and (b), (c), and (d) show the 100Ag, 150Ag, and 270Ag coatings respectively.

5.1 CURRENT DISTRIBUTION

The current density for the model was calculated in COMSOL. Figure 5.2 shows a graphical representation of the calculated current density distribution as a cross section of the terminal probe and surrounding silver coating. The current density was highest where the probe edges were in contact with the silver coating. It is evident from the graphical representations that the highest current density around the probe is found in the thinnest coating, 60Ag, Figure 5.2(a). The high current density areas diminish with increasing coating thickness, Figure 5.2(a) to 5.2(d), which can be directly related to lower resistance of the thicker coatings. The upper part of the contact area between the probe and the silver coating seems to have a slightly larger and redder area, implying that more of the current is passing through that area. This makes sense, as this area have the shortest distance to the other probe.

The plot of the current density between the two I-probes in Figure 5.3, shows that the COMSOL simulations gave a stable and continuous current distribution through the film. There were some irregularities in the area around the probes, at 0 and 38 μm, but this will have a small impact on the output since the voltage was measured around the 10 and 30 μm mark.

5.2 CONTACT PROPERTIES

The surface properties of the silver coating, together with data from an AgPS compression model[1], were applied to the resistance model. The model assumes a single sphere compressed between two gold plates. This was not directly transferable to the probe indentation. The probe pressure was for that reason applied as a sweep of different pressures, Table 5.1, within a range of ±25 MPa. This covered most of the early coating deformations observed in the model. The result from the COMSOL simulated sweep was that the resistance of the coatings did not change, but the amount of current increased with higher pressure. The surface properties were taken from the flattened AFM results, see Section 4.1.3.

1 The modeled pressure/indentation depth results will be part of Sigurd R. Pettersen Ph.D. thesis. [31]

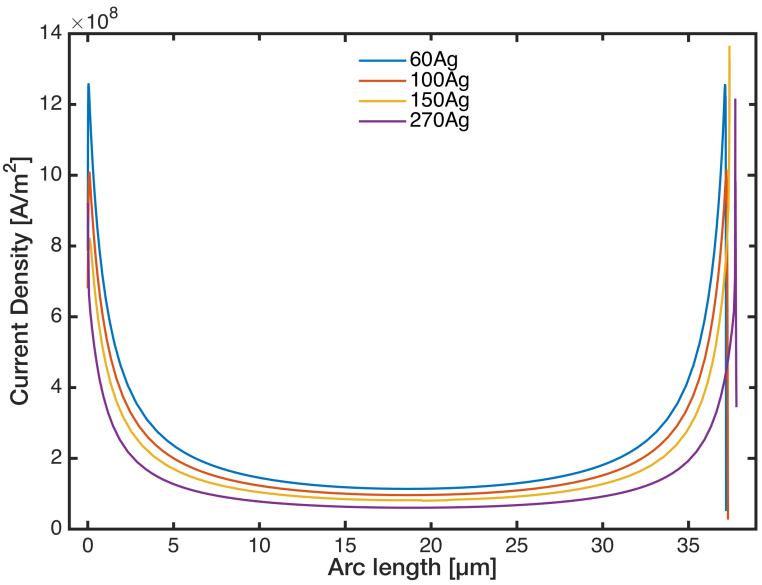

Figure 5.3: The modeled current density for the different AgPSs. The arc length on the x-axis goes from the uppermost intersection between the probe following the shortest way over the sphere circumference to the other probe as if the sphere was cut vertically in two. This gives the complete picture of the current density shown in Figure 5.2.

Table 5.1: The contact pressures used in the COMSOL models with corresponding indentation depths [31]. The minimum and maximum current density at one of the V-probes are also provided to see how the contact pressure sweep affects the COMSOL simulated currents.

Coating Thickness	60Ag	100Ag	150Ag	270Ag
Indention depth [nm]	46	77	122	153
Contact Pressure [MPa]	97	110	128	132
Current density min [A/m^2]	1.86E8	1.82E8	1.17E8	1.23E8
Current density max [A/m^2]	1.87E8	1.83E8	1.18E8	1.24E8

5.3 RESISTIVITY PREDICTION MODEL

The results from the COMSOL model can be used to predict the resistivity of an AgPS given a measured resistance with the four-wire method. By assuming the arc length between the V-probes are a constant $L_{arc} = 23\ \mu m$, for all measurements, the relation between the measured resistance, R_{4P} and the resistivity, $\rho^{\star}$, can be written as a

function, f, dependent on the coating thickness, t, and the sphere diameter, D, see Equation 5.1.

$$\frac{R_{4P}}{\rho^{\star}} = f\left(\frac{t}{D}\right)_{L_{arc}} \tag{5.1}$$

The model was based on the four thicknesses used, thus the model is not valid for t beyond the coating range of 60-270 nm. It should be safe to assume that the model should converge towards the bulk resistivity when the t is large and corresponding R_{4P} is low enough. This calls for a exponential equation that converges towards the ρ_{bulk} for silver. The minimum resistance in this model was set to $R_{min} = 0.015$, approximately 0.01 Ω lower that the 270Ag modeled resistance.

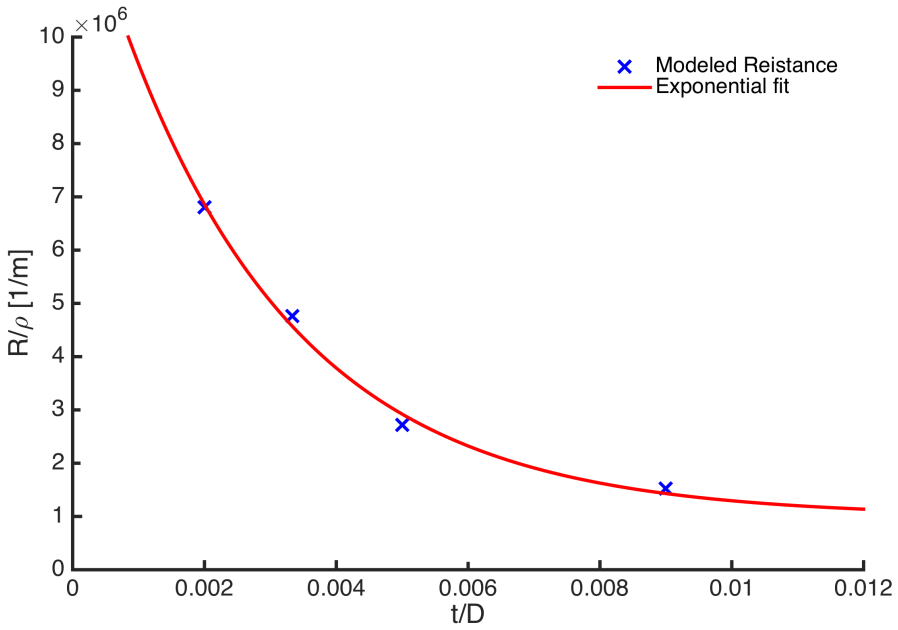

Figure 5.4: An exponential fit to the modeled resistances of the four coating thicknesses with constant V-probe distance of 23 µm. The exponential fit was based on Equation 5.2.

$$f\left(\frac{t}{D}\right)_{L_{arc}} = \frac{a}{\rho_{bulk}} e^{\left(-b \times \frac{t}{D}\right)} + \frac{R_{min}}{\rho_{bulk}} \tag{5.2}$$

Equation 5.2 was curve fitted with the Matlab *fit*[2] function with *NonlinearLeastSquare* method by changing the constants a and b. The graphical result of the fit, can be seen in Figure 5.4. The R-squared

2 See Matlab documentation at `http://se.mathworks.com/help/curvefit/fit.html`.

value, an indication on the goodness of fit (max value 1), was 0.99, which makes it a reasonably good fit.

$$\rho^{\star} = \frac{R_{4P}}{a\, e^{\left(-\frac{b\,t}{D}\right)} + R_{min}}\, \rho_{bulk} \tag{5.3}$$

By combining Equation 5.1 and 5.2, an expression for predicting the resistivity was given, Equation 5.3. By inserting the obtained constants $a = 0.187$ and $b = 371$, the complete resistivity prediction function was set, Equation 5.4.

$$\rho^{\star} = \frac{R_{4P}}{0.186e^{\left(-\frac{371t}{D}\right)} + 0.015}\, \rho_{bulk} \tag{5.4}$$

6 DISCUSSION

The present project has evolved during its progression and can now loosely be seen to consist of four parts: First, the development and optimization of a four-wire method for conducting electrical measurements on a spherical metal thin film. The question being whether it is feasible to use four micromanipulators to measure on a single AgPS? The second part has been to test the method on different AgPS coating thicknesses. Is the four-wire method more reliable than the two-wire, and what do these measurements show? The third part has qualitatively investigated some of the non-electric properties of the AgPS. Finally the measured results were applied in COMSOL Multiphysics to validate the results from the experimental measurements.

6.1 EXPERIMENTAL SETUP

Measurements of the electrical properties in micron sized electrical objects that are not connected to a circuit board, have not been documented to a large extent in literature. Investigations of planar thin films and coatings do exist [23, 33], but there are no reports available for similar measurements on spherical thin films. The miBots from IMINA TECHNOLOGIES enables the use of micromanipulators to do resistance measurements on single AgPS. They are thought to offer an environment where the electrical properties can be measured independently from mechanical deformation or contact area between spheres. However, the miBots or other parts of the experimental setup, have not been operated for this type of measurements before. The consequence being that everything from miBot handling, sample preparation, and probe design have to be developed and quality assessed, prior to the electrical measurements.

The miBot^{TM} BT-11-VP micromanipulators supplied by IMINA TECHNOLOGIES were used throughout this work. The handling of the miBots were simple and intuitive with the game pad, graphical user interface of the software, and live monitoring with the SEM. The very small step resolution was not utilized to its full potential, as both the

sphere and probes were in the micron regime. In addition, the force exerted from the smallest step sizes was often not enough to cause movement at all. The probes have no feedback loop that informs about the force being applied. Thus the silver film displacement and penetration depth had to evaluated through observation during probing and of the probe footprint.

Since a SEM was used to observe the spheres and probes, the AgPS had to be placed on an electrically conductive substrate to avoid charging, see Section 2.2.2.2. Earlier investigations dismissed both epoxy and carbon tape as a substrate adhesive as they both caused charging artifacts in the SEM images. The charging was avoided with the silver paint from AGAR SCIENTIFIC, but the adhesive properties was very poor[1]. The LEIT-C Carbon Cement (CC) proved a to have good conducting and adhesive properties. It was used as adhesive throughout the investigations presented in this study. The CC is viscous, which became a challenge when trying to distribute a thin and even layer on the Si substrate. The results being unwanted bumps or uncovered parts of the substrate. The CC viscosity also made it difficult to achieve a good connection area between the AgPS and the cement. Both dilution of the cement and mechanical pushing of the spheres were tried to address this issue. The latter caused some damage to the spheres, Figure 3.2, and was therefore discontinued. The result being that optimal adhesion was sacrificed in order to avoid damaged sphere coatings.

6.1.1 *Probes*

The polycrystalline tungsten (W) probes were easily milled down to the designated flat punch diameter of ~2 μm with the FIB. Similar flat punch size on both probes, gives better control over the indentation process. The lack of force control makes it important to have similar contact profiles from sphere to sphere in order to have comparable measuring conditions and results. The I-probes were always placed first. These probes had therefore the function of holding the sphere in place when the V-probes are connected in the four-wire setup. A larger flat punch area would have been better for holding the sphere in place, but they make poorer contacts with the coating as they are not always able to penetrate it, a problem especially for the two-wire measurements. Larger I-probes could also obstruct the placement of the V-probes in the four-wire setup, and could increase the chance of

1 These investigations were done in a preparation project for this thesis, and are therefore not fully documented here.

accidentally contacting the CC with the I-probes. The probe geometry is further discussed in Section 6.3.2.

The V-probes was made with the same geometry as the I-probes so that they could be used both for current and for voltage measurement. As demonstrated in Figure 4.8(b), a thinner set of probes was successfully introduced to measure the voltage in a four-wire setup of a 10 μm 150Ag. Using the normal set of probes proved not possible on such small features without short circuiting the other probes. The electrical evaluation placed the 10 μm spheres between the 30 μm 150Ag and 270Ag in resistance, which is reasonable considering the shorter silver coating distance covered between the V-probes.

6.2 RESISTANCE MEASUREMENTS

The main objective of this study have been to develop a method for measuring electrical properties of a single silver-coated polymer sphere. Two experimental approaches have been pursued: Two-wire measurements and four-wire measurements. They have both been carried out with the same experimental setup of miBots installed in a vacuum chamber of a FIB/SEM. The only change in setup being whether two or four wires/probes and miBots were connected and used for the measurement. The results from these measurements in Section 4.3 and Section 4.4, are however quite different.

6.2.1 *Two-wire Measurements*

The two-wire measurements have had challenges with inconsistency in the resistance output and in repeated measurements on the same particle. The resistance have also been much higher than predicted, Figure 4.10. Investigations of silver thin films [34], show that the resistance should be in the 0.1-0.01 Ω range.

Since a two-wire setup will measure the voltage drop over the whole circuit, a more accurate result is achieved by subtracting all the internal resistances contributing to the total measured resistance. In order to address the high resistance measured, the internal resistance of the system was measured, Section 4.3.1, and subtracted. The internal resistance was measured to be $R_{int,\,measured} = 6.41\Omega$, hence its contribution to closing in on the sub 1 Ω mark, was small (Figure 4.10 is corrected for $R_{int,\,measured}$).

As the resistance that contributes to the total measured resistance is neither from the coating of the spheres nor from the measuring circuit, it could be a feature of the contact between the probes and the AgPS. First looking at 60Ag, 150Ag, and 270Ag, and excluding

100Ag in Figure 4.10 and Table 4.3, there is a monotonic decrease in the resistance with increasing coating thickness. The thicker film seems easier to make contact with. This can be attributed to the larger silver coating deformation that causes more of the coatings's surface features to be plastically deformed, and thus increases the actual contact area. The standard deviation of these measurements are however large and overlapping, which gives this development a low credibility. The deviant 100Ag does not fit with this trend, as it has the lowest resistance mean and smallest deviation. Looking at the coating thicknesses isolated, gives no full answer to what contributes to the contact resistance. The contact resistance is therefore further discussed in Section 6.3.

The importance of knowing the contact resistance could also be discussed as the contact between a tungsten probe and the silver coating is not the same as a silver coating connection between spheres [35]. The results can for that reason not be directly transferred to which connections works best in a bulk sample of ICA with AgPS. Still, two-wire resistance can be used to say something about which coating thickness the developed experimental method works best with.

6.2.1.1 *Time Correlation*

The increase of resistance over time was observed to some extent in almost all two-wire measurements, like in Figure 4.9. The increase was observed in the estimated resistances when doing consecutive measurements on one sphere, and possible causes are discussed below.

Electromigration is a material transport effect caused by high direct currents traveling through thin metal films. In silver films, ions are pushed from the anode side towards the cathode causing a failure at the anode [36]. If a film is suffering from electromigration, holes should be seen near the anode and hillocks should appear near the cathode. But since the I-V sweep changes the current direction equally in both directions, the net movement of current is zero. This will also cancel out a potential thermal gradient from Joule heating. As a consequence electromigration is very unlikely, though a small accumulation of ions is still possible.

The increase of the resistance with time, was relative the regime of the resistance: If the first measurement begins at 104 Ω, it will increase to 130 Ω. Or if it begins at 22.8 Ω, it will increase to 25 Ω Figure 4.9. Joule heating is an effect that scales linearly with the resistance, and cause heat Q to develop where electrons collide with the atom lattice in the conducting material: $Q \propto I^2 \times R \times t$ [37, chap. 1.4]. At temperatures above 100 K, the resistivity of silver increase linearly with temperature [34]. This could cause a spiral where the

resistance induces heat and the heat causes larger resistance and so on.

However, the Joule heating scales with the square of the current, causing the Joule heating to be more sensitive to changes in current than resistance. At constant voltage, the effect of a change in current outweighs the effect of the corresponding resistance [37, chap. 1.4]. The relative Joule heating should then decrease with higher resistance, and the resistance should increase at a slower pace. This is observed in Figure 4.9.

Even though many of the measured spheres show increased resistance development with time, some do not. The 100Ag and 150Ag have spheres with resistances that either remain quite stable or that starts to decrease on the fourth/fifth consecutive measurement, in addition to the monotonic increasing cases. This questions whether or not the increased resistance are caused by the Joule heating, or why some spheres do not experience this effect in the same degree as others.

6.2.2 *Four-wire Measurements*

As the two-wire setup did not yield satisfying results in finding the resistance of the silver coatings, four-wire measurements were investigated. The four-wire setup involved two separate circuits attached to the same sphere, instead of one. The greatest challenge with this setup is to have all four probes in electrical contact with the sphere at the same time. Especially after placing the first pair of probes (the I-probes), the other pair is in danger of disconnecting the first pair by vibration or slight movement inflicted on the sphere. A method where the probes in turn are moved at a very short distance upon approaching the coating, helps to avoid this problem.

The big disadvantage of separating the V-probes from the I-probes, as performed in the four-wire measurements, is that only the voltage drop over a part of the sphere is measured. The current measured in the multimeter is distributed over the whole sphere. As seen in Figure 6.1, just a part of the current pass over the coating area probed. The coating constitutes of may parallel "resistances", meaning that the real resistance over the sphere is actually the combination of all these resistances. Consequently, the four-wire measurement do actually measure the slope of the voltage drop between the V-probes divided by the total current. Referring to Figure 6.1 and Ohm's law, Equation 2.9, the resistance would be larger than what is measured since the current between the V-probes are smaller. A more proper unit denomination should then be V/A in stead of Ω. The name and

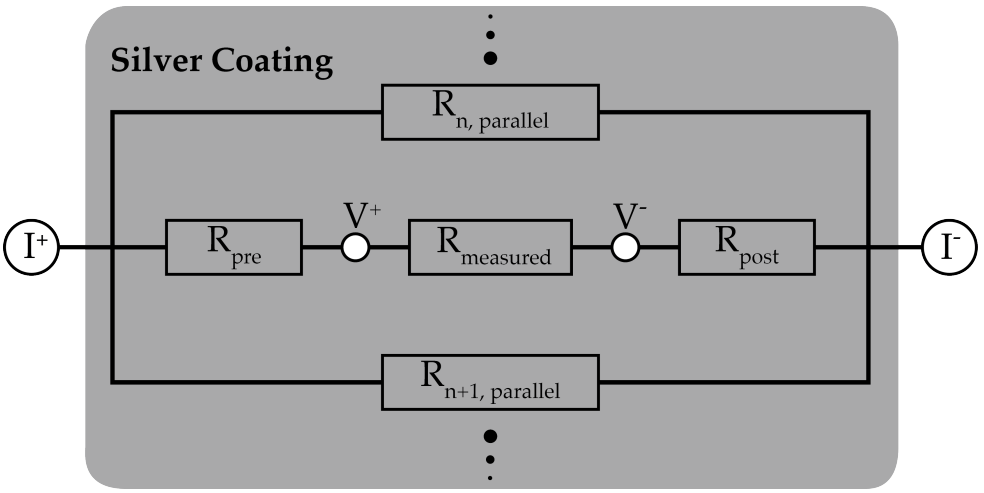

Figure 6.1: A simplified circuit outline for how the four-wire setup measures the resistivity. Only the potential drop in the coating between the V-probes are measured, but still related to all the terminal current that passes through the whole silver coating.

unit is however not changed in this study with reference to the discussion above.

6.2.2.1 *I-V Curves*

Compared with the less noisy lines of the I-V curves obtained from the two-wire measurements, see inserted I-V curves in Figure 4.9, the four-wire I-V curves look initially look as being of poorer quality. They are more fuzzy and most of them have a hysteresis loop. The four-wire method is measuring resistances that are 100 times smaller than what achieved with the two-wire. What is seen in Figure 4.11 is actually a result of a much higher resolution. The four-wire measurements show a hysteresis in the I-V curves, which makes it likely to be attributed to the silver coating or the new V-probes, since neither of them have been measured in the two-wire method.

Assuming that the hysteresis is caused by a charge accumulation in the system, a capacitor, it could be interesting to look a bit closer at the oxide layers in the silver coating and at the tungsten probes. According to literature [38], metal silver stored in air at 23°C, like the AgPS, have silver(II) oxide (AgO) present on the coating surface. AgO is a good conductor despite being an oxide, $\rho_{AgO} = 12\,\Omega\text{cm}$ [39], but can partly decompose to the much more insulating silver(I) oxide (Ag_2O) when subjected to heat an lower oxygen pressure, e.g. a vacuum chamber. Both the present AgO and the possible presence of Ag_2O could cause small capacitor like layers between the tungsten

probes and the silver coating [40]. Ag_2S are often present at silver surfaces, though not discussed here.

A oxide layer is also created on the tungsten probes when stored in air [41]. Tungsten(VI) oxide (WO_3) has also proved to have good charge capacity properties [42]. Since both Ag_xO and WO_3 have oxidation layers, though very thin, they could contribute to the hysteresis by creating small capacitors in the contacts or in the surface of the coating. However, the coatings are chemisorbed and so thin (~10 Å) that they under high enough contact pressure can be ignored [43, § 6]. Assuming this and the possibility of oxide capacitors, the hysteresis could be a result of too low contact pressure on one or more of the probes. The V-probes that are placed from the sides, see Figure 3.5, may not have as high contact pressure as the I-probes, thus creating a small oxide capacitor.

The calculated resistance from the I-V curves are not affected by the the hysteresis to a large extent. As demonstrated in Figure 4.12, the sphere that had a large hysteresis in the I-V curves still had a considerably lower resistance than the sphere with almost no hysteresis. The individual deviations between the spheres of the same thickness, seem to be larger than the effect of the hysteresis using the implemented resistance algorithm, Appendix B.

6.2.2.2 *Resistance*

The four-wire method was successful and provided measurements that were easy evaluate in with the Matlab script. As seen in Figure 4.12, consecutive measurements on the same sphere gave resistance with a very small deviation contrary to the two-wire measurements as discussed in Section 6.2.1.1. The mean of each AgPS was therefore used when comparing with the other spheres of the same coating thickness. The mean of these means was used to represent each coating thickness. The standard deviation between the spheres of the same coating thickness were very small, with the exception of the larger impact from the 60Ag, see Table 4.3 for details.

Just looking at the measured resistance in Figure 4.13, the 60Ag stands out from the development trend for the other three coating thicknesses. The sudden resistance jump up to 60Ag could indicate that the coating thickness is beginning to have its effect on the silver coating properties (size effects). As mentioned in Section 2.5.3, changes in the resistivity of silver thin films are reported to express itself by almost a linear increase when at the silver Electon Mean Free Path (EMFP) of 52 nm [11] or thinner. The fact that 60Ag is close to the EMFP threshold of 52 nm, may explain the sudden observed increase in resistance compared to the other spheres.

The deviations in V-probe distance between the coating thickness, see Table 4.3, do not seem to have influenced the resistance in a considerable way. The 150Ag have the smallest mean V-probe distance, the other coatings having a 15% or larger distance. This have not seemed to influence its relation to the other AgPSs, though the 150Ag resistance in theory should be lower. Hence, it is hard to tell from the data available whether or not the deviation in V-probe distance between the coating thicknesses are affecting the values in Figure 4.13.

The resistance marked in green in Figure 4.13, are from the COMSOL simulation model. They are all based on the same bulk conductivity. The change seen in resistance towards the tinner coating thickness is therefore a result of thinner silver coating, shorter indentation depth and lower contact pressure. The V-probe distance was set to match the mean of the measured distance for each type of AgPS, see Table 4.3. The reason for this was to make model conditions as similar to the experimental setup as possible, though it is not ideal to change so many parameters between the different model calculations. Either way, the model output follows the measured resistance quite well for the 270Ag, 150Ag, and 100Ag. The lower resistance in the simulation is expected as it is based on the bulk conductivity. The large difference in the 60Ag may again indicate a size effect taking place. The simulation is discussed further in Section 6.4.

6.2.2.3 *Resistivity*

The sphere geometry and how the current travels from the probes through the silver coating, makes it difficult to calculate the resistivity by a simple geometrical resistivity equation like Equation 2.8 of Ohm's law. Another approach, which makes use of the the simulated resistance results from COMSOL in relation to the experimental resistances, was derived in Equation 3.2 and 3.3. The results, see Table 4.4, are not all as expected.

Zhang et al. have investigated sputtered silver thin films on a p-Si substrate with a 200 nm Si_2O and 10 nm/15 nm TaN/Ta barrier layer [24]. The resistance was found by four-point-probe sheet resistance measurements, and the resistivity by the use of Equation 2.8. Their result is plotted together with the resistivity found in Table 4.4. Even though the two silver coatings are prepared by different methods and substrates, a comparison should be able to tell something about the new four-wire method used for measuring the AgPS.

Figure 6.2 plots the resistivity obtained from the AgPS measurements together with the sputtered silver films from Zhang et al. By comparing the two, the following observations are made:

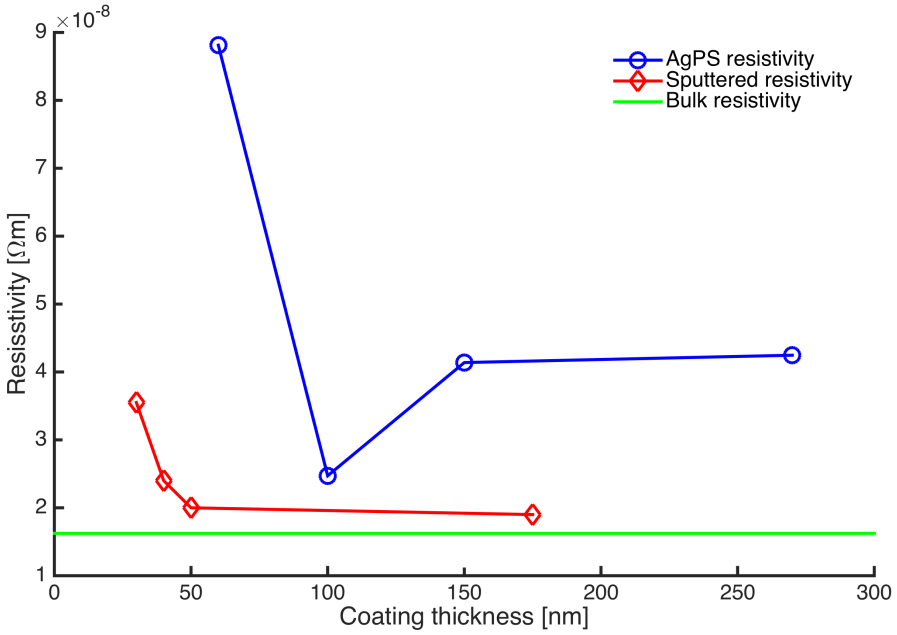

Figure 6.2: The estimated AgPS resistivity calculated from the experimental/simulation relation, the blue line. The red line show the sputtered silver film resistivity of a flat substrate, from Zhang et al. [24]. The green line is the silver bulk resistivity.

1. The 60Ag size effect seems premature.
2. The 100Ag are closest to the resistivity reported by Zhang et al.
3. By extrapolating the results from Zhang et al. both 150Ag and 270Ag should be lower than 100Ag, developing in the same way as the four-wire experimental resistance in Figure 4.13.

First, the high resistivity of 60Ag could be caused by measurement artifacts. For the sputtered thin film, the size effect likely caused by the EMFP of silver at 52 nm, begin to affect the resistivity first for the films thinner than 50 nm. It could be that the actual thickness of the 60Ag silver coating is thinner than reported by the manufacturer or has poorer quality enabling the EMFP effects for a seemingly thicker coating. In addition, considering the silver grains in the coating which have a high probability of being smaller than the EMFP. There are most probably differences in the morphology and topology between the sputtered and chemically deposited silver films. The 60Ags had a RMS roughness of 13.1 nm compared to the 45 nm thick sputtered silver film with a RMS roughness of 1.31 nm [24]. As a consequence, the continuous silver coating of 60Ag could be closer to the EMFP and justify part of the large resistivity increase.

The second and third observation points out a clear weakness of combining a novel experimental method with a quite simple model

simulation. The 100Ag, that has a measured resistance closest to the model, gives the best resistivity estimate. Using Equation 3.2 for calculating resistivity in the COMSOL model gave results that differ from experimental results. A short distance between the COMSOL model and the experimental results, see 100Ag in Figure 4.13, yields a good fit to the sputtered resistivity in Figure 6.2. Imagine if the results from the 150Ag had been closest to the simulated resistance. Then would 150Ag end up with the resistivity closest to the measurements on the sputtered coating. This does not mean that the simulation model is the only factor to blame for the strange resistivity development seen in Figure 6.2; the experimental results do also have its flaws as earlier mentioned.

6.3 THE COATING SURFACE

To get a better understanding of the electrical properties and behaviors of the AgPS, their surfaces have been studied by SEM and AFM. The SEM offers great details of the AgPS surface, and the possibility to avoid the damaged or failed coatings under the resistance measurements, Figure 3.1. By taking a closer look at the spheres' individual coatings, it became obvious that the same coating procedure can create quite different morphologies and topographies, see Figure 4.1. The obvious being that the thicker coatings have bigger surface features.

The 60Ag coating, Figure 4.1(a), looks like a surface of Ag grains in a monolayer. It gives the impression of catching a glimpse of the underlying PMMA core at some of the grain boundaries. Probing could easily break the coating at the grain boundaries or the thin film can at places be discontinuous which would cause a higher resistance. The grains are not as visible on the 100Ag, giving the impression of a more continuous film, thus a lower resistance. The small holes observed in Figure 4.1(b), are sometimes present in the 60Ag as well, but have not been found to cause a lower resistance.

A different type of structure is seen in the 150Ag coating, Figure 4.1(c). The bright grains of good BSE feedback from the SEM could, if assuming only silver present, be small crystalline grains of silver, see Section 2.1.1. This type of coating was occasionally observed in both 100Ag and 150Ag, without being able to document an impact on the resistance. The thickest coating, Figure 4.1(d), had no problems with coating coverage, but the large surface features could cause problems in achieving a good enough contact area, hence increasing the resistance between contacting spheres. The thickness have however been reported to be mainly an asset in AgPS bulk adhesives [5].

6.3.1 *Surface Properties*

The AFM offers a great way to quantify surface properties with its precise, quantitative mapping of the surface topology. The information being a vital part of the simulation model in COMSOL, but also to understand how current flows from the probes to the AgPS surface. A challenge have been to acquire good data from the spherical surface of the AgPS. In post processing, the flattening method, Section 3.6.2, have been used to eliminate the surface curvature and reveal the details in the topography, see Figure 4.3. It is hard to say if this has deteriorated the AFM data. However, the change in RMS surface roughness after flattening was substantial, especially for 150Ag and 270Ag, Figure 4.4. Comparing with the SEM pictures of the same coating thicknesses, Figure 4.1, the 150Ag surface look much more similar to the 100Ag than to the 270Ag which supports the AFM flattening result. Still, this one example do imply that all the AFM data flattenings resulted in a surface topology closer to reality.

The RMS surface roughness develops as expected with larger roughness with thicker coating, the RMS surface slope in contrast, Figure 4.5, follows another pattern. The 60Ag surfaces almost have as steep slopes as the 270Ag. However, the data obtained from the 60Ag were suffering from artifacts in the form of sudden high peaks. These are caused by the AFM tip not being able to follow the surface and are not representing the actual surface. These artifacts were not observed in any of the other coatings, hence the actual RMS surface slope of the 60Ags is probably lower.

In the two-wire measurements, the 100Ag spheres deviated somewhat from the trend of decreasing resistance with increasing coating thickness. Since most of the resistances measured in the two-wire setup are believed to be attributed to the contact resistance, could the surface topography in the contact area prove interesting. The 100Ag have the lowest RMS surface slope and roughness, Table 4.1, providing a good contact environment for the probes. The 270Ag have on the other hand both the highest RMS surface roughness and slope, at the same time as having the second lowest resistance. Therefore, looking at the two-wire resistance in relation to the surface properties could be a relative measure of the quality of the probe indentation.

As the contact resistance in theory is omitted in the four-wire measurements, the surface topography should have little influence on these results. The large standard deviation in the resistance for the 60Ag are probably more a result of larger individual differences in a thin coating such as 60 nm.

6.3.2 *Mechanical Properties*

As mentioned in Section 4.1.2, the different coating thicknesses give varying experienced mechanical properties upon probe indentation. The difference of 210 nm between 60Ag and 270Ag change the mechanical properties from viscoelastic to a plastic metal [44], the 270Ag not being particularly influenced by the polymer core. From the current setup, the 100Ag gave the impression of being the easiest spheres to measure. The combination of a silver film thick enough not to break easily, and the elastic properties of the polymer core proved a good match for the 2 μm flat punch probe. This raises the question whether the flat punch area should be more custom sized for the different thicknesses. A larger flat punch area (+1 μm diameter) would maybe favor the thinnest 60Ag coating, distributing the indentation force over a larger area e.g. lower the pressure. The thicker coating, especially, 270Ag could be favored by at a smaller flat punch probe, that could easier penetrate through the rough and more metal-like properties.

6.4 SIMULATION

The experimental four-wire setup applied to the AgPS is a novel method. It has therefore been important to verify the results. Simulating the setup using model calculations was a obvious choice, as no complimentary experimental setup exists. A simulation model is a theoretical approximation, but the question is whether or not it is a good approximation. As earlier mentioned, the simulation model fits quite nicely to the coating thickness dependent resistance in Figure 4.13. The large deviation for the 60Ag spheres is probably a result of both experimental difficulties and that they maybe should have redefined physical properties in the COMSOL model to incorporate beginning silver thickness size effects.

The distribution of domains, the mesh, and the general electrical physics have performed as it should (see discussion further down), the weakest link being the electrical contact between the probes and sphere coating. The CMY model applied at the contacts seem to work well, but the input parameters are not completely trustworthy: First, the probe contact pressure should be modeled simultaneously as an indentation. Furthermore, the silver microhardness found experimentally for the different coating thicknesses to accommodate the changing mechanical properties should be incorporated in the model, Section 6.3.2. Finally, a more thorough AFM investigation of the surface properties to rule out artifacts form the AFM measurements. That be-

ing said, this is foremost an experimental investigation, the simulation giving supportive information to the main objective.

6.4.1 *V-probe Distance*

The simulation model was tested and found to be good at evaluating the different coating thicknesses, but it should also be able to model different distances between the V-probes. Experimental four-wire measurements on the 100Ag for three different V-probe distances were performed for reference. They showed an increased resistance with increasing V-probe distance, Figure 4.14, as expected. The corresponding COMSOL simulation followed the same increasing trend. The experimentally measured and model calculated resistance based on the longest V-probe distance, had the largest deviation. This could be a sign of the model not being able to simulate the higher current density areas with as much precision as the lower current density areas further from the I-probes. However, it could also be a variation in the experimental resistance that causes the extra deviation. Either way, the model clearly adapts to the different V-probe distances.

6.4.2 *Current Distribution*

The current density profiles extracted from the path of the V-probes in the model Figure 5.2, shows a continuous distribution without jumps or irregularities except for the beginnings and ends where the I-probes are situated. The voltage is however measured in the continuous part of the current distribution, where the model and sufficient mesh resolution have provided a good current profile, and is an example of COMSOL's sophisticated model abilities.

The 2D cross sections of one I-probe in contact with the coating Figure 5.3, give an interesting insight into which part of the probe that is used to transfer current. Looking at the probes, most of the current pass through the edges of the probe, the interior of the probe contact area is not utilized. It would be interesting to investigate if a flat plate in horizontal contact with the same circumference would have the same current transferring abilities. Such a design would at lest be easier to handle in an experimental setup.

The contact pressure sweep, mentioned in Section 5.2 did not result in a significant difference in the simulated resistance, as expected by a four-wire measurement. As for the current density, an increase with increasing pressure was observed, Table 5.1. This indicates that the applied CMY model works well, taking the surface topography from the AFM and the surface pressure into account when simulating the

current. Note that the 150Ag have a lower current density than 270Ag because the V-probe is further away from the I-probe, see Table 4.3. Regarding the pressures used, it is important to remember that they are based on another simulation. In order to best relate the probe pressure to the resistance and surface roughness, a multiphysics simulation combining both mechanical and electrical nodes, should be performed. This may result in the model resistances being closer to the experimental.

6.4.3 *Resistivity Prediction Model*

A prediction model, Section 5.3, based on the COMSOL simulation model was made to have an easy way of predicting the resistivity given the V-probe distance of 23 µm. The only required input, is the measured resistance by a four-point measurement technique and inserting the AgPS diameter and coating thickness. This is a very simplified equation that completely ignores the experimental data. Nevertheless, it should give an indication to the degree of resistivity. At least for the three thickest coatings who had a quite good fit between the experimental and the model, Figure 4.13.

The prediction model is based on a exponential fit to the simulated resistances in COMSOL, Figure 5.4. The exponential fit was chosen due to its simplicity and good fit. The model is not tested on AgPS with a sphere diameter other than 30 µm, so its reliability is poor in regard to size of the spheres.

7 CONCLUSION

Conductive adhesives with silver-coated polymer spheres are a promising alternative to lead-containing solders that are being phased out of many applications. The development and commercialization of isotropic conductive adhesive (ICA) with silver coated polymer spheres (AgPSs) are dependent on the performance of single AgPS conductivity and finding the optimal performance. Optimization is made possible by a method for resistance measurements on single AgPS. The four-wire method proposed in this study proves to be feasible; the obtained experimental results are to a large extent supported by complimenting COMSOL model calculations.

7.1 EXPERIMENTAL SETUP

The method used for two- and four-wire probing of a single AgPS was made possible by the miBot micromanipulators from IMINA TECHNOLOGIES setup in a vacuum chamber with a SEM column for in situ observation and manipulation. The handling of the miBots are simple and intuitive, but they offer no force or indentation depth control. The spheres were dispersed on a Si substrate with Carbon Cement (CC) as an conductive adhesive. The CC viscosity was a challenge in trying to get a good adhesion area with the spheres, and was partly overcome by diluting of the cement.

The FIB was used to mill the tungsten probes down to a flat punch area of ~2 μm. The probe size was found to give best support for the 100Ag, thinner coatings could benefit from a larger area and thicker coatings from a smaller. Simulations revealed that the major part of the current is transfered through the circumference of the I-probe, this could favor other probe geometries with larger circumference to area ratio. The V-probes proved not to have the same size and geometry dependence when tested with smaller probes as very little current pass through them.

7.2 SILVER COATING RESISTANCE

The two-wire experimental measurements resulted in the mean resistances summed up in Table 7.1. All the measurements is two to three magnitudes larger than expected after removing the measured internal resistance in the circuit, $R_{int,\,measured} = 6.41\Omega$. The resistance do not scale monotonic with the coating thickness, 100Ag having the smallest mean resistance of 17.9 Ω. The measured resistance are most probably caused by the contact resistance which changes with both the surface slope and roughness combined with how well the probe geometry and indentation "fits" with the surface features.

The observed trend of the resistance increasing with time when performing multiple measurements on the same sphere, is suggested to be caused by Joule heating. The heat raises the resistivity of the silver which leads to increased resistance. But since the trend is not observed for all spheres, a change in the contact area between measurements could also be a cause.

Table 7.1: A summary of the mean resistances from the two- and four-wire experimental measurements. The apparent resistivity is also included.

Coating Thickness	60Ag	100Ag	150Ag	270Ag
2W Resistance [Ω]	91.1±52.7	17.9±9.2	38.0±19.7	29.4±17.5
4W Resistance [Ω]	0.604±0.228	0.118±0.012	0.096±0.016	0.079±0.011
App.Resistivity [Ωm]	8.81E-8	2.47E-8	4.14E-8	4.42E-8

The more cumbersome four-wire setup gave measurements that were in the anticipated resistance regime for a thin silver film. The four-wire method omits the contact and internal resistance, but most of the silver coating as well. Therefore, the resistance should in theory be higher than measured as the current is smaller between the V-probes. The measured resistances decreases with increasing coating thickness, and the standard deviation is small between the particles, as seen in Table 7.1. Furthermore, the time correlation observed in the two-wire measurements is not present in the consecutive measurements on one AgPS. The four-wire setup with miBots have proved itself as a reliable method for resistance measurements.

The hysteresis observed in most of the I-V curves obtained with the four-wire setup, are an interesting artifact, even though their impact on the resistance result in most cases are negligible. An oxide layer on the silver coating and/or on the tungsten probes are proposed to act like a capacitor, but this has not been investigated.

The four-wire measured resistance in the 60Ag is considerably higher than for the other silver coatings. This could be a size effect caused by the thin silver film is closing up on the silver EMFP of 52 nm, causing a linear increase in resistivity. The 60Ag has then a thinner conductive silver layer than reported from the manufacturer or the silver coating may not cover the sphere continuously. There could also be a weakness in the four-wire setup when measuring coatings this thin.

7.3 RESISTANCE SIMULATION

A simulation model of the four-wire setup was successfully implemented in COMSOL Multiphysics. The model can predict changes in resistance due to the coating thickness and the V-probe distance. The modeled resistance is lower than the experimental resistance, as the bulk resistivity is used throughout the simulations. Though AFM investigations of the coatings were included in the model, a simultaneous mechanical simulation with better coating property constants would improve the model even further.

A prediction of the AgPS resistivity was made by combining the experimental and simulated resistance, called the apparent resistivity Table 7.1. The resulting resistivity did not develop as expected, but were within an order of magnitude. For future reference, a resistivity prediction model was made from the simulation results to predict the resistivity given the coating thickness, sphere radius, and four-wire resistance.

8 FURTHER WORK

This master's thesis was performed with the main objective to develop and test a method for measuring electrical properties on spherical thin films of silver, or more precise, the silver coated polymer sphere (AgPS). For further work, there are multiple measures regarding the experimental setup that can be performed to improve the four-wire technique and the input in the COMSOL models:

- The sample preparation could be improved further to ensure better adhesion and dispersion of the spheres.
- A more standardized protocol for the experimental setup detailing optimal V-probe distance and I-probe placement. This would give more consistent experimental results.
- The I-probe geometry should be more tailored to the different films, both different sizes of circular flat punch probes as well as probe geometries with a larger circumference should be tested. Here would both COMSOL simulations and experimental investigations be useful.
- The parameters applied to the electrical contact between the probes and the sphere in the COMSOL models could be improved by doing a more thorough AFM investigation and by finding the microhardness of the different spheres by mechanical investigations with a nanoindenter.
- The existing COMSOL model should be supplemented with a mechanical module for a more realistic implementation of the indentation of the probes.

More work is needed to improve the COMSOL models for the understanding of resistivity in spheres, and how it could be calculated from geometrical considerations. This could be achieved by a better understanding of the experimental setup and a further development of the COMSOL model, as mentioned above.

The hysteresis seen in the four-wire I-V curves, Figure 4.11, should also be investigated further. Are the oxides from the silver and tungsten responsible for the charge accumulation, or is it from other parts of the system? Little is known about the capacitance of silver oxide or tungsten oxide thin films, which yet is to be documented in the literature. A reductive treatment of the spheres before four-wire measuring, would be interesting when investigating a possible oxide effect.

The silver to silver contact properties is important for the spheres when in bulk adhesives. The four-wire setup in combination with patterned substrates etc. to get the AgPS aligned next to one another, could make this possible.

This method could also have interesting applications in the semiconductor or biology field. I.e. the measurement of geometrically challenging micro circuits or electrical properties of neuron cells.

BIBLIOGRAPHY

[1] Yi Li, Daniel Lu, and C P Wong. *Electrical Conductive Adhesives with Nanotechnologies*. Springer US, Boston, MA, 2010. ISBN 9780387887838. (Cited on pages 1 and 2.)

[2] S. Jain, D.C. Whalley, M. Cottrill, H. Kristiansen, K. Redford, C. B. Nilsen, T. Helland, and C. Liu. Electrical properties of an isotropic conductive adhesive filled with silver coated polymer spheres. pages 1–7, 2011. (Cited on pages 1 and 2.)

[3] Helge Kristiansen and Tore Helland. Isotropic Conductive Adhesive. 2013. *Patent* US 2013/0323501. (Cited on page 1.)

[4] Hoang-Vu Nguyen, Helge Kristiansen, Rolf Johannessen, Erik Andreassen, Andreas Larsson, Nils Hoivik, and Knut E. Aasmundtveit. Temperature dependence of mechanical properties of isotropic conductive adhesive filled with metal coated polymer spheres. pages 639–644, 2011. ISBN 978-1-61284-497-8. (Cited on page 1.)

[5] S. Jain, D. C. Whalley, M. Cottrill, T. Helland, H. Kristiansen, K. Redford, and C. Liu. The effect of coating thickness on the electrical performance of novel isotropic conductive adhesives prepared using metallised polymer micro-spheres. In *IEEE*, pages 796–802. IEEE, 5 2013. ISBN 978-1-4799-0232-3. (Cited on pages 2 and 70.)

[6] Hoang-Vu Nguyen, Erik Andreassen, Helge Kristiansen, and Knut E. Aasmundtveit. Die shear testing of a novel isotropic conductive adhesive-epoxy filled with metal-coated polymer spheres. 3(7):1084–1093, 7 2013. ISSN 2156-3950. (Cited on page 1.)

[7] Hoang-Vu Nguyen, Erik Andreassen, Helge Kristiansen, Rolf Johannessen, Nils Hoivik, and Knut E. Aasmundtveit. Rheological characterization of a novel isotropic conductive adhesive - epoxy filled with metal-coated polymer spheres. 46:784–793, 4 2013. ISSN 02613069. (Cited on page 2.)

[8] Jarmo Maattanen. Contact resistance of metal-coated polymer particles used in anisotropically conductive adhesives. *Emerald Group Publishing, Limited*, 15(1):12, 2003. ISSN 09540911. (Cited on page 2.)

[9] Masahiro Inoue and Katsuaki Suganuma. Effect of curing conditions on the electrical properties of isotropic conductive adhesives composed of an epoxy-based binder. *Emerald Group Publishing, Limited*, 18(2):40–45, 2006. ISSN 09540911. (Cited on page 2.)

[10] Hong Zhou, Sen-Jiang Yu, Yong-Ju Zhang, Miao-Gen Chen, Zhi-Wei Jiao, and Ping-Zhan Si. In situ electric properties of ag films deposited on rough substrates. 93(1):18–26, 1 2013. ISSN 0950-0839. (Cited on page 2.)

[11] Haoyan Wei and Hergen Eilers. From silver nanoparticles to thin films: Evolution of microstructure and electrical conduction on glass substrates. 70(2):459–465, 2 2009. ISSN 00223697. (Cited on pages 2, 19, and 67.)

[12] PJ Goodhew, FJ Humphreys, and R Beanland. *Electron Microscopy and Analysis*. 2001. ISBN 0203184254. (Cited on pages 5, 6, 7, 9, and 10.)

[13] LA Gianuzzi and FA Stevie. *Introduction to Focused Ion Beams*. Kluwer Academic Publishers, Boston, 2005. ISBN 0-387-23116-1. (Cited on pages 5, 7, and 8.)

[14] Nan Yao. *Focused Ion Beam Systems*. Cambridge University Press, Cambridge, 2007. ISBN 9780511600302. (Cited on pages 7 and 8.)

[15] Jacques Gierak, Ralf Jede, and Peter Hawkes. Nanofabrication with focused ion beams. In *CRC Press*, pages 41–84. CRC Press, 2 2012. ISBN 978-1-4200-9052-9. (Cited on page 8.)

[16] David B. Williams and C. Barry Carter. *Transmission Electron Microscopy*. Springer US, Boston, MA, 2009. ISBN 978-0-387-76500-6. (Cited on page 10.)

[17] Yang Leng. *Materials characterization: introduction to microscopic and spectroscopic methods*. Wiley, Singapore, 2008. ISBN 978-0-470-82298-2. (Cited on pages 10 and 11.)

[18] Bede Pittenger, Natalia Erina, and Chanmin Su. Mechanical property mapping at the nanoscale using peakforce qnm scanning probe technique. 203:31–51, 2014. (Cited on page 12.)

[19] Bruker. Nanoscope analysis 1.50 user manual, 2014. (Cited on page 13.)

[20] Maximilian Erlbeck. Probing the electronic properties of p-doped gallium arsenide nanowires. Master's thesis, NTNU, 2014. (Cited on page 15.)

[21] Michael B Heaney. *Electrical Measurement, Signal Processing, and Displays*, volume 18 of *Principles and Applications in Engineering*. CRC Press, 7 2003. ISBN 978-0-8493-1733-0. (Cited on pages 15, 16, 17, and 18.)

[22] Paul G Slade. *Electrical contacts: principles and applications*. Number Second edition. Taylor & Francis, Boca Raton, 2014. ISBN 9781439881316. (Cited on pages 17 and 19.)

[23] Shuji Hasegawa, Ichiro Shiraki, Takehiro Tanikawa, Christian L Petersen, Torben M Hansen, Peter Boggild, and Francois Grey. Direct measurement of surface-state conductance by microscopic four-point probe method. 14(35):8379–8392, 9 2002. ISSN 0953-8984. (Cited on pages 18, 19, and 61.)

[24] W. Zhang, S.H. Brongersma, O. Richard, B. Brijs, R. Palmans, L. Froyen, and K. Maex. Influence of the electron mean free path on the resistivity of thin metal films. 76(1-4):146–152, 10 2004. ISSN 01679317. (Cited on pages 19, 68, and 69.)

[25] Pramond D Desai, TK Chu, Ho M James, and CY Ho. Electrical resistivity of selected elements. 13(4):1069–1096, 1984. (Cited on page 19.)

[26] Roger W. Pryor. *Multiphysics Modeling Using COMSOL®: A First Principles Approach*. Jones & Bartlett Publishers, 2009. ISBN 1449656064. (Cited on page 20.)

[27] Jacob Fish and Ted Belytschko. *A First Course in Finite Elements*. John Wiley & Sons, Ltd, Chichester, UK, 4 2007. ISBN 9780470510858. URL `http://doi.wiley.com/10.1002/9780470510858`. (Cited on page 20.)

[28] M M Yovanovich and E E Marotta. *Thermal spreading and contact resistances*. John Wiley, 2003. (Cited on page 21.)

[29] M.G. Cooper, B.B. Mikic, and M.M. Yovanovich. Thermal contact conductance. 12(3):279–300, 3 1969. ISSN 00179310. (Cited on page 22.)

[30] N.P. Kobelev, Ya.M. Soifer, R.A. Andrievski, and B. Gunther. Microhardness and elastic properties of nanocrystalline silver. 2(5): 537–544, 9 1993. ISSN 09659773. (Cited on page 34.)

[31] Sigurd R. Pettersen. *Unpublished*. PhD thesis, Norwegian University of Science and Engineering, 2016. (Cited on pages 34, 35, 41, 57, and 58.)

[32] Ronald E Walpole. *Probability & statistics for engineers & scientists*. Number 8th ed. Pearson Prentice Hall, Upper Saddle River, N.J., 2007. ISBN 0-13-204767-5. (Cited on page 49.)

[33] EZ Luo, S Heun, M Kennedy, J. Wollschläger, and M. Henzler. Surface roughness and conductivity of thin ag films. *Physical Review B*, 49(7):4858–4865, 2 1994. ISSN 0163-1829. (Cited on page 61.)

[34] DB Tanner and DC Larson. Electrical resistivity of silver films. 166(3):652–655, 2 1968. ISSN 0031-899X. (Cited on pages 63 and 64.)

[35] S. Jain, D.C. Whalley, M. Cottrill, H. Kristiansen, K. Redford, S. Helland, T. Helland, E. Kalland, and C. Liu. Factors affecting conduction in novel isotropic conductive adhesives filled with silver coated polymer spheres. pages 1–7, 2013. (Cited on page 64.)

[36] H.M. Breitling and R.E. Hummel. Electromigration in thin silver, copper, gold, indium, tin, lead and magnesium films. 33(4):845–852, 1 1972. ISSN 00223697. (Cited on page 64.)

[37] Alexandra von Meier. *Electric power systems: a conceptual introduction*. IEEE Press, Hoboken, N.J., 2006. ISBN 0470036427. (Cited on pages 64 and 65.)

[38] V. A. Lavrenko, A. I. Malyshevskaya, L. I. Kuznetsova, V. F. Litvinenko, and V. N. Pavlikov. Features of high-temperature oxidation in air of silver and alloy ag-cu, and adsorption of oxygen on silver. 45(9-10):476–480, 9 2006. ISSN 1068-1302. (Cited on page 66.)

[39] Bryan E. Breyfogle. Electrodeposition of silver(ii) oxide films. *The Electrochemical Society*, 143(9):2741, 9 1996. ISSN 00134651. (Cited on page 66.)

[40] B. D. Cahan, J. B. Ockerman, R. F. Amlie, and P. Rüetschi. The silver-silver oxide electrode. *The Electrochemical Society*, 107(9): 725, 9 1960. ISSN 00134651. (Cited on page 67.)

[41] Anna Warren, Anders Nylund, and Ingemar Olefjord. Oxidation of tungsten and tungsten carbide in dry and humid atmospheres. 14(5-6):345–353, 1 1996. ISSN 02634368. (Cited on page 67.)

[42] A. Azens, C. G. Granqvist, E. Pentjuss, J. Gabrusenoks, and J. Barczynska. Electrochromism of fluorinated and electron-bombarded tungsten oxide films. *AIP Publishing*, 78(3):1968, 8 1995. ISSN 00218979. (Cited on page 67.)

[43] Ragnar Holm and Else Holm. *Electric contacts: theory and application*. Number 4. compl. rewritten ed. Springer, Berlin, 1967. ISBN 978-3-642-05708-3. (Cited on page 67.)

[44] Tore Helland. Experimental and numerical study on the nano-mechanical properties of polymer particles. Master's thesis, Norwegian University of Science and Technology (NTNU), 2008. (Cited on page 72.)

A

TIPS AND TRICKS

This section has gathered a few tips and tricks which could come in handy when doing two- and four-wire measurements with the miBot setup presented in this study.

APPROACHING THE PROBES The probe approaching should be done stepwise. The I-probes should be placed first, since they are furthest down. Upon approaching the film, switch probe between each step to get an even indent from both sides. When the I-probes have locked onto the sphere, use the same approach to place the V-probes directly above.

COATING THICKNESS It is important to note that different thicknesses needs different approaches. The thicker coating needs a somewhat harder approach to penetrate into the silver and make a good electrical contact. The thinner and more ductile coating demands a gentler approach.

FOUR-WIRE TROUBLESHOOTING If the four-wire measurements do not behave as expected, do two-wire tests on both pairs to locate any bad connectivity. Amping up the current during this test could also help, see next tip.

IDLE PROBES Probes that have been idle for some weeks, have not been used, or have some small residues are performing much better after some two-wire measurements at higher currents (5-50 mA). (This should not be done on 60Ag, which do not handle such high currents.)

ALIGNMENT To avoid time consuming transportation of the probes when loaded in the vacuum chamber, they should be aligned approximately above the area of the sample where the AgPSs to be investigated are. As showed in Figure 3.4.

DOCUMENTATION Take pictures of all your measurements. It can be very useful to see the probe placement, distance, and possible movement of the probes when evaluating the corresponding measurement data.

B

MATLAB SCRIPT

The code used to evaluate the data from the I-V measurements is listed below, Listing B.1. The code is implemented in Matlab and should be self explanatory with the help of the comments. The function imports takes in number if measurements, and creates names standarized file names. The I-V curves are then imported, before the resistance is calculated with a linear regression to the least mean squares. The calculated resistances are set as output of the equation together with plots of the I-V curves and the resistance.

Listing B.1: The code for calculating and plotting all the results from one particle.

```
function [r] = results(measurements)
%Input: Total number of indents from one particle
    %Returns the calculated resistances

    particle= 'A';   % particle name
    coating = '100'; % paticle coating thickness

%----Preallocating Variables----------
files = cell(1,measurements);
xtik= cell(1, measurements);
r=zeros(measurements,1);
x=zeros(measurements,1);

%---------Create filenames------------
    for i=1:measurements
        if i>9
        files{i} = strcat(particle,'_',coating,'nm_01',
            char(38+i), '.dat');
        xtik{i} = strcat('01', char(38+i));
        x(i)=i;
        else
        files{i} = strcat(particle,'_',coating,'nm_00',
            char(48+i), '.dat');
        xtik{i} = strcat('00', char(48+i));
        x(i)=i;
        end
```

```
25      end
26
27     OC={}; %Failed measurements to be omitted
28
29     %Resize variables if measurements are omitted
30     s=size(OC);
31     measurements=measurements-s(2);
32     files=setdiff(files,OC);
33     x=x(1:measurements);
34     r=r(1:measurements);
35
36 %---------------------------------
37 %  Import Function
38 %---------------------------------
39      function [ V, I ] = datImport( filename )
40          %datImport imports .dat files form the IV-sweep
41          %Remember to import filnames with brackets!
42
43      struct=importdata(filename);    %the data is imported
            as a structure
44      data=struct.data;   %Separates the data from the text
45      I=data(:,2);    %Returns data in the right variable
46      V=data(:,1);
47      end
48
49 %---------------------------------
50 %  Resistance Function
51 %---------------------------------
52      function [ R ] = resistance( V,I )
53      %resitance takes a linear fit of the IV-curve and
            finds the resistance
54
55      p=polyfit(V,I,1);   %Makes a linear regression to the
            I and V variables
56                      %and returns the slope
57      plot(V,I);
58
59      R=1/p(1); %The reisistance is found by the inverse of
            the slope
60      end
61
62 %---------------------------------
63 %  Final Evaluation Function
64 %---------------------------------
65     function [ R ] = evaluate( filename )
66      %Imports measurement from file
67      %   Returns the resistance of that measurement
68
69      [V,I] = datImport(filename);
70
71      R = resistance(V,I);
72      end
```

```
73
74 %-----Plot IV curves----------------
75     figure;
76     hold on;
77     for j=1:measurements
78         r(j)=evaluate(files{j}); %import IV curves and
               resistances
79     end
80
81     xlabel('Voltage (V)','FontSize',14);
82     ylabel('Current (A)','FontSize',14);
83     title(strjoin({'IV curves of particle', particle,
           coating, 'nm'}),...
84          'FontSize',14);
85     legend(xtik,'Location', 'Southeast');
86     hold off;
87
88 %-----Plot Resistance measurements----
89
90     figure;
91     plot(x,r, '+');
92     xlabel('Measurement number','FontSize',14);
93     ylabel('Resistance (\Omega)','FontSize',14);
94     title(strjoin({'Resistance as a function of
           measurement number for particle',...
95          particle}),'FontSize',14);
96     legend('Calculated resistance');
97     set(gca,'XTickLabel',xtik);
98     set(gca,'XTick',[1:measurements]);
99 end
```